Akademie věd České republiky

Teze doktorské disertační práce
k získání vědeckého titulu "doktor věd"
ve skupině věd fyzikálně - matematických

Structure and Properties of Exotic Nuclei using Radioactive Nuclear Beams

název disertace

Komise pro obhajoby doktorských disertací v oboru jaderné, subjaderné a matematické fyziky

Jméno uchazeče ... Zdeněk Dlouhý

Pracoviště uchazeče ... ÚJF, AVČR, Řež

Místo a datum ... Praha, Listopad 2006

Contents

1 Introduction

1.1 Motivation

The study of the properties of extremely neutron- or proton-rich nuclei of light elements is considered as an important and exciting research topic in modern nuclear physics. For a given mass number A, the proportion of neutrons and protons that corresponds to the most stable configuration is determined by the combined action of the various phenomena that govern nuclear binding. In this way the stability region is presented on the Chart of the Nuclides, on which each bound nucleus is plotted as a function of N and Z. Not far from stability these nuclei generally convert into stable nuclei by β-decay of neutrons into protons or vice versa. It is the weak interaction which is responsible for this transmutation, which explains the very long times required for β-decay processes, spanning from a few milliseconds to millions of years.

Far away from stability the limits of nuclear existence are reached, where one or more nucleons are no longer bound. An unbound nuclear system disintegrates quasi-instantaneously (in a time interval of the order of 10^{-21} s). The locus of points on the nuclear chart joining nuclei that are unbound to proton(neutron) emission in the ground state is called the proton(neutron) drip line. These drip lines form the edges of the nuclear chart. About 280 stable or very long-lived nuclear species are found on the Earth but, according to current estimates, from 5000 to 7000 bound nuclei should exist in the Universe. Only 2000 have been synthesized and observed to date, but very little information is available about these unstable nuclei. Their lifetimes, masses or sizes are often unknown, their modes of radioactive decay have seldom been identified and information on their excited levels is very limited or nonexistent. The interest in this field has been stimulated by the fact that nuclei lying near the drip lines - the boundaries of the nuclear stability - have revealed new features that considerably differ from those of normal nuclei lying close to the valley of stability.

One way of probing properties of a nucleus is to make it undergo nuclear reactions. In the case of the stable nuclei, one usually makes a target containing the nuclei of interest and bombards it with a beam of suitable particles. Exotic nuclei, however, are unstable and rare and thus cannot be formed into a target. Hence these nuclei have to be used in a form of exotic beams and directed onto the target of stable nuclei. Radioactive Nuclear Beams (RNB) as well as great progress advanced in detector developments thus open up a vast field of research with inestimable potential for new discoveries.

Except for the lightest elements up to nitrogen the boundary of the experimentally reached region of neutron-rich nuclei is still far away from the neutron drip line, and this fact leaves a great challenge for experimentalists for years to come. Not only this urges on the development of new powerful methods to produce and detect such nuclei but it also ensures that the progress in diverse nuclear models will remain active. The experimental investigation of both the light nuclei and the quasistable nuclear systems having an anomalous N/Z ratio lying near the boundary of the particle stability is of particular interest since the extreme cases of a nucleon configuration give us the unique chance to test the nuclear models on nuclei where models should be more sensitive to

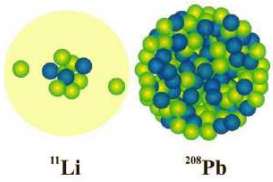

Figure 1: A scale illustration of the size of the orbits of weakly bound neutrons in the heaviest, rare lithium isotope, compared with the size of a lead nucleus.

the choice of the nuclear potential parameters.

Nowadays, the exploration of exotic, short-lived nuclei having large neutron-to-proton imbalance has demonstrated that the "universal" ideas of nuclear properties are in fact not correct. Fig.1 illustrates how unusual these exotic forms of nuclei called "halo" can be compared to nuclei studied so far. The size of the orbits of weakly bound neutrons in the heaviest, rare lithium isotope, is comparable with the size of a lead nucleus. The figure illustrates that standard assumptions, such as that the size of a nucleus depends only on the total number of neutrons and protons, are not always valid. Thus light nuclei are a testing ground for probing inter-nucleon forces. The simplest nuclear system having a two-neutron halo is ^{6}He with two loosely bound neutrons that orbit around a compact alpha particle. But take away one neutron or the alpha particle and the system will immediately fall apart. The two extra neutrons interact together as a pairing interaction, and make this system of an alpha particle and two neutrons stable. Pairing of nucleons is a common, yet not well understood feature of nuclei and halo nuclei provide new insights into its origin and nature.

Even though the number of undiscovered bound nuclei is very large, we are able to make single big steps by studying just few specific nuclei. These nuclei act as milestones in establishing the new effects that arise in extreme conditions of isospin asymmetry. By rephrasing this, the nuclear models as we see them today are evolved and based on the available experimental data, which lead to the conclusion that in many cases the model parameters are simply insufficient in predicting nuclear features that appear closer to the drip line.

So the first example of a characteristic feature of nuclei near the drip line is an existence of a halo or a little tightly bound skin structure [Tan85] which appeared in this region to proclame the decoupling of the neutron and proton matter. The search for further and heavier nuclei possessing this feature is extending. The understanding of the decoupling of the proton and neutron matter distributions is the first step on the way to solve the astrophysical problem of neutron stars.

Another example of a quite new phenomenon that has appeared in neutron-rich region is the magicity breaking at the neutron numbers N=8 and 20. It concerns the nuclei which have well known large energy shell gaps appearing in analogy with the periodical system of elements. These large gaps appear in nuclei with neutron numbers N=2, 8, 20, 28 ... that are known as "magic numbers". The nuclei having magic structure both in Z and N are called doubly-magic and possess the extra stability. Despite of large stability of lightest doubly-magic nucleus ^{4}He (Z=2, N=2) the next doubly-magic nucleus ^{10}He (Z=2, N=8) was found to be unbound by the

Riken [Kor94] and Berlin [Ost94] groups after the search being carried out for more than 30 years [Ste88, Dlo92]. This nucleus, if bound, would possess the highest N/Z ratio among all known nuclei. The instability of neutron-rich doubly-magic ^{10}He is a very strange feature which could lead to changes in shell closures of neutron-rich nuclei. Among recent results exploring the double magicity of neutron-rich isotopes in the C-Mg region we should mention the experiments leading to the particle instability of neutron-rich oxygen isotopes $^{25-26}$O [Fau96, Gui90] on one hand as well as the evidence for new bound nuclei ^{31}Ne [Sak96] and ^{31}F [Sak99] on the other.

Moreover, further magicity breaking has also been observed at the N=20 shell closure where the existence of a so-called "island of inversion" has been pointed out [Thi75]. The neutron rich Na and Mg nuclei around N = 20 were found to be more bound than predicted by a spherical closed-shell prescription. However, large scale shell model calculations have demonstrated that some configurations arising from the excitation of a pair of neutrons are more strongly bound than configurations with spherical shapes. The isotopes of ^{30,31,32}Mg are the key nuclei located at the border of this region. A number of recent experiments using a variety of advanced probes has been focused on the structure of these exotic nuclei. The progressive development of a prolate deformation that was revealed in this region [Mot95] instead of the spherical stability which was expected on the basis on the magicity of the neutron number N=20, has been a serious puzzle for long time. In this region the shell model configurations are strongly rearranged. In particular, the ^{30}Mg and ^{32}Mg nuclei are expected to exhibit coexistence of spherical and intruder (deformed) configurations, yet it is not clear how to classify the excited states observed at low excitation energy into members of these configurations.

The new information that would better characterize the excited states and the search for a candidate for the intruder 0^+ state in these nuclei is highly desirable. In the present time we carry out a very active research program in the heavy Mg region using complementary techniques at the ISOLDE facility at CERN. Despite many experimental attempts on these exotic nuclei there remains a number of issues still to be resolved.

The disappearance of the neutron magic number N=20 in the island of inversion and the particle stability of ^{31}F could be due to the strong mixing between the $d_{3/2}$ and $f_{7/2}$ states [Pov94]. This effect may lead to the larger deformations and could enhance the binding energies of new neutron-rich nuclei at the drip line. Thus we may also expect that the drip line for the fluorine-magnesium isotopes which is very important since it limits the particle stability in this region [Mit97] could move far beyond the presently known boundaries.

Studies of short-lived nuclei far from β-stability offer a unique test of those aspects of the many-body problem that depend on the isospin degrees-of-freedom. The challenge to microscopic theory is to predict and provide reliable calculations of the properties of these exotic systems. For medium- and heavy-mass nuclei, the objective is a universal energy density functional, that will enable a description of finite nuclei (static properties, collective states, large-amplitude collective motion), as well as extended asymmetric nucleonic matter (e.g. as found in neutron stars). When extrapolating from ordinary stable nuclei to extended nuclear matter found in very

neutron-rich nuclei, a number of effects have to be taken into account. The diffuseness of the neutron surface implies that the gradient terms in the density functional are as important in defining the energy relations, as those depending on the local density. When approaching the one-nucleon drip line, pairing correlations become as important as mean-field effects. Pairing correlations modify the asymptotic properties of single-nucleon densities and, therefore, the dependence of weakly-bound systems on the detailed features of effective nuclear interactions is much stronger than in ordinary stable nuclei. Such a microscopic calculation necessitates a simultaneous description of particle-hole, pairing, and continuum effects - a challenge that could only be addressed very recently by mean-field methods.

In addition to the intrinsic nuclear structure interest, many properties of nuclei far from the valley of β-stability are crucial for a deeper understanding of the nuclear processes governing stellar nucleosynthesis. From a theoretical point of view, the principal goal is to achieve a consistent picture of structure and reaction aspects of weakly bound and unbound nuclei, which requires an accurate description of both the many-body correlations and the continuum of positive-energy states and decay channels. A coherent description of the relation between scattering states, resonances and bound states in the many-body wave function necessitates a close interplay between methods of nuclear structure and reaction theory. This mutual cross-fertilization presents an opportunity to open a new era in the theory of loosely bound systems.

1.2 Exotic beam production

The study of all phenomena mentioned above obviously requires to make available to the physicists Radioactive Nuclear Beams (RNB) facilities which play a crucial role in this field of physics and cannot be substituted by any other methods. Till 1985 the access to nuclei near the border of β-stability was practically unreachable due to large difference in the number of identical nucleons (neutrons or protons) between stable target nuclei and the new nuclei near the drip line. This difference cannot be overcome by any light projectile.

With the advent of RNB facilities the situation has changed dramatically. RNB have proved to be a useful tool for studying nuclei far from the valley of stability. There are two principal methods which exist for the production of RNB. The so called ISOL method which is applied in CERN uses protons accelerated to 1 GeV to bombard a heated thick ^{238}U target. The spallation products diffuse to the ion source where they are accelerated to 60 keV. Then they are separated by a magnetic field, and used in different kinds of experiments. In the other named in-flight (or fragmentation) method, the primary stable ion beams accelerated by sophisticated facilities up to an energy of several hundreds A.MeV undergo the fragmentation on a thin target and the reaction products of relatively high energy are separated by fragment separators and exploited either to study the properties of the fragments themselves or to initiate other types of nuclear reactions.

The properties of exotic nuclei are studied using RNB produced at cyclotron facilities at GANIL - Caen (France), FLNR, JINR -Dubna (Russia), Michigan State University (USA) , RIKEN (Japan) and for relativistic RNB at GSI (Germany).

At GANIL, the secondary beams are usually obtained by stable beams of ^{13}C, ^{18}O, ^{36}S and ^{48}Ca accelerated to energies up to 100 A.MeV that undergo the fragmentation on various targets. The fragmentation products are separated and purified by doubly-achromatic fragment separator LISE3 [Ann92] or directly analyzed by energy loss spectrometer SPEG.

1.3 This thesis

In this work, an information on nuclear structure is reached by different approaches. We start from elastic and inelastic scattering, nuclear reactions, beta and gamma decays, and go on to binding energies and nuclear level schemes analyzed in the shell model framework. The scattering and reaction data are treated by different frameworks used to analyze various nuclear reactions while experimental data concerning the structure are used as the input parameters for the shell model analyses, which results in the contribution to the basic physical quantities such as nucleon interactions, for specific range of nuclei.

This thesis consists of 22 publications dealing with various aspects of nuclear structure. The papers collected in the thesis cover the period since 1992 till now. Most of them were published in the well-known international physical journals, based on the experimental data measured and analyzed on cyclotron facilities and experimental equipments built at GANIL, France with help of NPI ASCR.

The general outline of this thesis is composed of four topics.

The first theme – the study of anomalities in nuclear matter including the nucleon halo or skin structure of neutron-rich [A1, A2, A4] and proton-rich [A3, A5, A6] nuclei discussed in Sec. 3. There are also included the measurements of reaction cross sections of different light ions on proton target [A7] and of the charge and mass deformation of ^{30,32}Mg [A8].

The second theme presented in Sec. 4 concentrates on the particle stability near the drip line. The stability of doubly-magic nucleus ^{28}O[A9, A10], the drip line location for Ne, Na and Mg [A11], and their spectroscopic properties [A12] have been investigated.

The third topic (Sec. 5) has been dedicated to the detailed investigation of nuclei in the neutron-rich region from Z=6 up to 20 since both the neutron-rich doubly-magic nuclei ^{10}He [Kor94, Ost94] and ^{28}O [A9, Sak99] have been found to be unbound. The precise measurements of nuclear masses [A13] allows us to obtain two-neutron separation energies which are known to be the effective tool to point out the location of nuclear shells. The analyses of two neutron separation energies has enabled us to reveal the changes of shell closures [A14, A15] of light neutron-rich nuclei and to establish new magic number N=16 for nuclei in this neutron-rich region [A16, A17, A18].

The last topic (Sec. 6) concentrates to the confirmation of our new results using another novel method, the in-beam gamma-ray spectroscopy[A19, A20, A21, A22].

2 Theoretical Basis

The basic milestone to determine exactly the properties of nuclear matter is a proper understanding of the nucleus in terms of nucleon-nucleon (NN) interaction. At its most fundamental level, this requires a description of the nucleon in terms of quarks and gluons; at present we believe the appropriate theory to be the quantum chromodynamics (QCD). The NN interaction can, in principle, be fully determined within QCD but our knowledge of QCD is still too limited to yield an adequate interaction that can be used subsequently as an input for the description of a many-nucleon system. Another complication arises because the free NN interaction is, for nucleons in a nucleus, modified to take account of the surrounding nuclear medium.

The description of a nucleus cannot use directly the description of neutrons and protons in terms of interacting quarks. The atomic nucleus is a complex, many-body system bound by the strong interaction, and one simplifies the problem by using the concept of effective forces. Medium effects arising from the action of all the other nucleons on one of them are simulated using an effective interaction which is based on the determination of several parameters deduced from what we know about a few key stable nuclei. This is why most of our understanding of the nucleus comes from experimental investigations of stable nuclei. This effective NN interaction is kept constant for all nuclei and its general form is suggested by underlying microscopic but non-relativistic considerations. Alternatively, a relativistic mean-field theory can be formulated in terms of effective fields that are mediated by carrier bosons, mesons.

The approaches mentioned so far are mean-field theories which treat the nucleus as an ensemble of nucleons that are moving independently in a potential generated by the other nucleons and among which no additional correlations are considered, apart from pairing. However, current experiments with RNB extend our knowledge of nuclei away from the valley of stability towards the drip lines and one scientific justification for them is that they provide additional tests of effective microscopic theories. A more comprehensive description of the nucleus must go beyond the mean-field approximation: only then the full variety of its spectral properties, collective rotations and vibrations, giant resonances, its single-particle excitations, etc. conceivably might find some interpretation.

2.1 Shell model

If we look at gross nuclear properties, such as nucleon separation energies, we find that these vary smoothly in most region of the nuclear chart. However, at certain specific nucleon numbers, the so called magic numbers (2, 8, 20, 28, 50, 82, 126), we observe discrete jumps. These are the fingerprints of the nuclear shell structure. The magic nuclei are understood in terms of the nuclear shell model and its associated shell gaps.

The nuclear shell model is currently the most complete microscopic model of the atomic nucleus. Starting with the mean-field basis, a shell model calculation is based upon a subset of single-particle states together with their interaction via an effective two (or more) body Hamiltonian. In many cases the single-particle energies can be inferred from an experiment. The experimental energies for all magic nuclei can be semi-

quantitatively described in terms of Hartree-Fock models [Bro98]. These models are necessary for the extrapolation of single-particle properties of nuclei far from stability. Doubly-magic nuclei – those that have a magic number for both protons and neutrons are crucial for the understanding of nuclear structure.

The closed-shell property of the doubly-magic nuclei provides a good zeroth-order wave function which can be systematically improved upon by using perturbation theory. Starting with a zero-particle zero-hole (0p-0h) closed shell, the structure of the closed shells themselves can be systematically improved by the mixing of 2p-2h and higher excitations. The renormalized G-matrix [Kuo68] provides a starting point for the two-body Hamiltonians, but the agreement with an experiment can often be greatly improved by empirical modifications of the two-body matrix elements.

The experimental signatures of magic numbers are the presence of a discontinuity in the one- and two-nucleon separation energies, and a relatively high energy for the first-excited state in even-even nuclei (usually 2^+) at the magic number – a feature characteristic of most doubly-magic nuclei which is significantly higher than that at all of the neighboring even-even nuclei. In doubly-magic nuclei, such as ^{40}Ca (Z=20, N=20), this excitation energy reaches very high energy of about 3.9 MeV. There are many more such nuclei with Z $<$ 30 which will be discussed here. For those nuclei beyond Z $\geq$ 30 there are only three such nuclei, ^{100,132}Sn and ^{208}Pb.

These shell-gap effects in the binding energies give rise to the dramatic isotopic changes in the formation of elements in stellar events where intense neutron fluxes exist. The rapid neutron capture, the so called r-process, in competition with the beta decay is responsible for formation of heavier nuclei and the role of magic nuclei is to slow down the r-process at the magic neutron numbers. So the element abundances are related to shell effects in very neutron-rich nuclei which have not yet been studied experimentally.

The general form of the nuclear Hamiltonian is

$$H = \sum_{i=1}^{A} T(i) + \sum_{1=k<l}^{A} W(k,l), \tag{1}$$

where $T(i)$ denotes the kinetic energy term and $W(k,l)$ stands for the two-body-interaction between nucleons k and l. The starting point of the shell model is the single particle model [Hax49], based on an idea of an independent nucleon orbiting freely in a spherically symmetrical central potential $U(r)$ produced by all the other nucleons inside the nucleus. The Hamiltonian, describing such an independent-particle motion in a nucleus with the total number of A nucleons, is given by

$$H^{(0)} = \sum_{i=1}^{A} \left[T(i) + U(r_i) \right], \tag{2}$$

where $U(r_i)$ is the single particle potential. The realistic shell model Hamiltonian includes also the particle-particle correlations, represented by the so-called residual

interaction described by the Hamiltonian $H^{(1)}$so that the total Hamiltonian, H, consisting of the independent particle motion and residual interaction, is given by

$$H = H^{(0)} + H^{(1)} = \sum_{i=1}^{A}[T(i) + U(r_i)] + \left[\sum_{1=k<l}^{A} W(k,l) - \sum_{i=1}^{A} U(r_i)\right], \tag{3}$$

which can be eventually applied to the many-body Schrödinger equation, $H\Psi = E\Psi$. By considering $H^{(1)}$ as a perturbation the energy of the eigenstate, E_Γ, is therefore given by

$$E_\Gamma = \langle \Phi_\Gamma^{(0)} | H^{(0)} + H^{(1)} | \Phi_\Gamma^{(0)} \rangle = \sum_{k=1}^{A} e_{a_k} + \langle \Phi_\Gamma^{(0)} | H^{(1)} | \Phi_\Gamma^{(0)} \rangle, \tag{4}$$

where the letter Γ includes the total spin J and isospin T, the first terms e_{a_k}, results from the single-particle energies and the second term from the residual interaction.

In the real shell model calculations the nuclear states are not represented by pure shell-model states, but they are their linear combination. Thus the complete Hamiltonian and the mixed wave-function finally result in a matrix form with matrix elements H_{lk}. The diagonal matrix elements result from the unperturbed Hamiltonian, $H^{(0)}$, and two–body interactions. The solution of a nuclear energy spectrum is obtained finally by diagonalization of the energy matrix.

Shell model calculations are performed always in a limited configuration space, which consists of a restricted set of single particle states outside an inert core, often a doubly-magic nucleus. A direct consequence of this truncation is that the residual interactions have to be considered as effective interactions and the appropriate choice for such an NN interaction is not trivial.

2.1.1 Monte Carlo Shell model

Although the nuclear shell model provides the benchmark for an understanding of properties of nuclei, it must be stressed that calculations within its framework are extremely complex and time-consuming. The conventional shell model diagonalization for a complete one-major shell has been possible only up to the *sd*-shell, since the dimension of the Hamiltonian matrix becomes too large to be diagonalized for larger shells. In order to overcome this difficulty, the Monte Carlo Shell model (MCSM) [Hon96, Ots98] has been proposed based on the Quantum Monte-Carlo Diagonalization (QMCD) [Hon95, Miz96] method. In the MCSM calculation, basis states are generated stochastically and are either adopted or discarded according to its importance for lowering the total energy. The Hamiltonian matrix is then diagonalized in a subspace spanned by these selected basis states. In that sense the MCSM calculations can be characterized as an "importance truncation" scheme. Since the MCSM utilizes a general deformed bases, we can consider the whole model space. By using the MCSM it is possible to carry out shell model calculations in the pf and higher shells with reasonable accuracy.

2.2 Elastic scattering and direct nuclear reactions

Theoretical description of nuclear reactions is based on various models and approaches. Different approaches are used not only for the description of various types of reactions but also for the description of the one and the same reaction. This arises from the fact, that the task on the interaction between nuclei is connected with multichannel and many-body problems, and their solution is not trivial. In most cases only the knowledge of the structure of projectile and target nuclei is not sufficient to solve the problem, and also the interaction between incident particles are also necessary. Therefore different approaches for the description of nuclear reactions vary in degree of their accuracy and the model assumptions laid in their basis.

The two techniques most often used to interpret and analyzed experimental data on direct reactions are the coupled channels (CC) and distorted-waves (DW) methods. In the CC method, we obtain a solution of a relatively small set of coupled equations that results with the small number of terms, and the truncation implies the use of an effective Hamiltonian and interaction. When the method is applied to elastic plus inelastic scattering, and all basis states belong to the same partition we refer to it as CC. When rearrangement is being considered, and the states from more that one partition are present, the coupled reaction channels (CRC) take place.

When the amplitude for a nonelastic event is calculated to first order in the coupling interaction, whereas the elastic scattering is treated more completely, and usually with use of an optical potential, we have the method of distorted waves. If the coupled equations of the corresponding CC or CRC problem are solved to first order in the coupling interaction, the distorted-wave Born approximation (DWBA) takes place. However, we should retain a distinction between this and the more usual procedure whereby optical potentials are chosen to reproduce the measured elastic scattering.

At low energies two heavy ions (HI) interact only through their Coulomb fields, and can scatter elastically or inelastically with a Coulomb excitation. Nuclear interaction can only take place if the two ions energy, E_{cm}, in their center of mass system is high enough to overcome the Coulomb barrier, and thus the minimal distance between the two interacting ions is $r_{min} < R_N$, where R_N is the distance where the nuclear interaction disappears. However, such a description is only qualitative and the full treatment must take account of the quantum mechanical nature of the process.

2.2.1 Folding model

In this approach it is desirable to relate the nucleus – nucleus potential to the nucleon-nucleon interaction. The nuclear potential may be obtained by integrating an NN interaction over the matter distributions of the two colliding nuclei. This approach is called the folding model and has been reviewed by Satchler and Love [Sat79, Sat83]. Initially, calculations of the folded potentials were of the single folding (SF) form. In this approach a phenomenological nucleon-nucleus potential $U_{1N}(\mathbf{r})$ describing the interaction of a nucleon with nucleus 1 was integrated over the density distribution $\rho_2(\mathbf{r})$ of nucleus 2

$$U_F(\mathbf{R}) = \int d\mathbf{r}_2\, \rho_2(\mathbf{r}_2) U_{1N}(\mathbf{R} - \mathbf{r}_2). \tag{5}$$

However, for heavy-ion scattering it was found that this approach overestimated the strength of the potential by a factor of about 2 and therefore the full double-folding (DF) form had to be used. Then the NN interaction, V(r), is integrated over both density distributions

$$U_{Fi}(\mathbf{R}) = \int d\mathbf{r}_1 \int d\mathbf{r}_2\, \rho_1(\mathbf{r}_1)\rho_2(\mathbf{r}_2) V_i(\mathbf{R} - \mathbf{r}_1 + \mathbf{r}_2). \tag{6}$$

In both equations $\mathbf{R}$ is the vector between centers of ions and $\mathbf{r}_{1,2}$ are relative vectors of nucleons. The SF form may be viewed as a special case with $\rho_1(r) = \delta(r)$ and may be calculated as such.

In addition to its use for the elastic scattering the folding model may also be employed to calculate transition potentials for the inelastic scattering and other reaction processes if a suitable interaction is integrated over the appropriate transition densities of the two nuclei.

2.2.2 Optical model of elastic scattering

One of the most widely used approaches to describe the elastic scattering of two nuclei is based on the optical potential (OP). Customarily phenomenological Woods-Saxon forms used for both the real and imaginary parts of OP are applied for angular distribution analysis in the well-known form

$$V(r) = -V_v f(x_v) - iW_w f(x_w) + i4a_d W_d \frac{df(x_d)}{dr} + \tag{7}$$

$$+(\frac{h}{m_\pi c})^2 (V_{s.o.} + iW_{s.o.}) \frac{1}{r} \frac{df(x_{s.o.})}{dr}\ .\ (\mathbf{l}\ .\ \sigma) + V_c(x_c),$$

where the radial dependence is taken in the Woods-Saxon form

$$f(r) = \left[1 + exp\left(\frac{x_i - r_i A^{1/3}}{a_i}\right)\right]^{-1}. \tag{8}$$

Usually, the primary optical model analysis of HI scattering is performed using phenomenological six (or more) parameters of Woods-Saxon potentials. However, a satisfactory microscopic understanding of the scattering process can be achieved if one relates OP to a fundamental NN interaction through DF approach by folding this interaction with the nuclear-matter distributions of both the projectile and the target nuclei [Sat79, Sat83]. During the last two decades HI elastic scattering data were successfully predicted using the DF potential as the real part of OP, while the imaginary potential was fitted in a phenomenological form. However, an anomalous behavior of potential was noticed by [Sat79, Sam97] for weakly bound nuclei, where the

folded potential had to be reduced by a renormalization coefficient ($N_V = 0.5 - 0.6$) in order to reproduce the data. This anomaly was attributed to the effect of the breakup of the loosely bound nuclei and the factor N_V could be completely accounted for by considering an explicit coupling of the elastic channel with the low-lying breakup channels [Sam97]. As the incident energy increases, the breakup channel and coupling effect usually decreases and the value of N_V approaches 1.0.

In the folding model analysis the choice of the NN interaction is very crucial. Different effective NN interactions, M3Y [Ber77], S1Y [Sat79], KH [Kny81] and the effective interaction of Jeukene, Lejeune and Mahaux [JLM77] are used to derive these potentials. Successful predictions of the observed cross-sections were obtained by these potentials. The M3Y and S1Y interactions provided the best predictions of the data. The KH interaction came next in this respect. The JLM interaction presents a very powerful tool to describe the interactions of light nuclei analyzed, particularly, at the backward angles. The M3Y and S1Y potentials showed similar behaviours for the required renormalization factors and energy dependence of the volume integrals.

3 Anomalies in Nuclear Matter Distribution

The interest to the light neutron-rich nuclei has arisen for the most part by the experiment on the matter distribution of ^{11}Li by Tanihata [Tan85] , whereby the weak binding of the last one or two neutrons has led to the formation of an extended distribution well beyond that expected on the basis of systematics. Hansen and Jonson [Han87] have proposed a "neutron halo" model of ^{11}Li to account for these observations. In the case of ^{6}He the two neutrons are more tightly bound and the structure is called "neutron skin".

The structure of nuclei far from stability and close to the particle drip lines is very rich. In neutron-rich nuclei, in particular, exotic phenomena include the weak binding of the outermost neutrons, pronounced effects of the coupling between bound states and the particle continuum, regions of nuclei with very diffuse neutron densities and the formation of neutron skin and halo structures.

Weakly bound systems provide a sensitive test of the nuclear force, and the neighbourhood of the drip lines provides a unique proving ground for the development of our understanding of these interactions which are of fundamental importance. It can be shown how the three-body system changes as we make the transition across the drip line. On the bound side of the drip line lies a variety of rather intriguing substructures. Amongst them there are the Borromean nuclei which possess the property that none of the two-particle subsystems are bound, and it requires three-body correlations to bind the system. An example of such a nucleus would be ^{6}He (^{4}He+n+n). Equally, it is possible to have 3-body systems in which only two of the constituents are bound, for example ^{6}Li (^{4}He+n+p) where the n and p are bound but the ^{4}He+n (^{5}He) and ^{4}He+p (^{5}Li) subsystems are not. The comparison between these nuclei and Borromean systems allows a detailed understanding of the 3-body correlations to be achieved. Not only this is essential in the study of the bound 3-body states. Also the resonances in the unbound 2-body constituents and those in the unbound 3-body systems are highly

needed.

In the first experiments when the intensities of RNB were very low only the interaction cross section of loosely bound nuclei with different targets could be measured since a high value of its cross section enabled to produce the data of sufficient statistics. Later, these data have been complemented with data of the transverse and parallel momenta measurements that have provided further support for the neutron-halo hypothesis. Nevertheless, although these experiments give information about the extent of the neutron cloud and the degree of correlation between the two extra-core neutrons, they are unable to provide detailed information about the proton and neutron distributions in halo nuclei.

Such information can, in principle, be obtained from measurements of the elastic scattering angular distributions or the dissociation and breakup reactions of radioactive nuclei. In this way, it would be possible to test various theoretical descriptions of halo nuclei. Moreover, neither the elastic scattering nor the dissociation and breakup reactions of radioactive nuclei were carried out in that time. Therefore, we tried to obtain the new information on nuclear halo and skin structure of light nuclei using these methods. We used the secondary beams obtained by from stable beams of ^{13}C and ^{18}O accelerated to energies up to 50 A.MeV that undergo the fragmentation on various targets. The fragmentation products are separated and purified by doubly-achromatic fragment separator LISE3 [Ann92] consisting of two dipoles with an achromatic wedge and a Wien velocity filter. The selected ion beam is analyzed and directed onto the secondary target to perform different types of reactions. Intensities of separated isotopes have reached up to 1000 pps with purities better than 98%, that have been sufficient to perform not only the elastic scattering experiments but also experiments on dissociation, breakup and reaction cross section of several exotic nuclei. In the first experiments, the incident angle of incoming ions has been defined by the entrance collimator, later it has been measured by position-sensitive PPAC detectors. Their mass and charge have been identified by bi-dimensional spectra obtained by various combinations of measured parameters, e.g. their time of flight, TOF, energy losses in Si-transmission detectors, dE, and residual energy, E, in the thick Si or other detectors. The schematic setup for the elastic scattering experiments is presented in Fig.2.

3.1 Nuclear halo and skin structure

As we have mentioned above the nuclear halo and skin structure which can be studied by a great span of reactions has been the subject of growing interest in nuclear physics. However, the use of these methods for the case when one of nuclei is radioactive is rather complicated. The complex nature of the projectile causes that a number of new reactions occur, and also when the projectile fuses with a target nucleus one has to consider the special features due to the large angular momentum carried by the projectile.

At low energies two heavy ions interact through their Coulomb fields and nuclear interaction can only take place if their energy E_{cm} is high enough to overcome the Coulomb barrier. In such circumstances the interaction shows the semiclassical features which makes it possible to give an overall description in terms of impact parameter b.

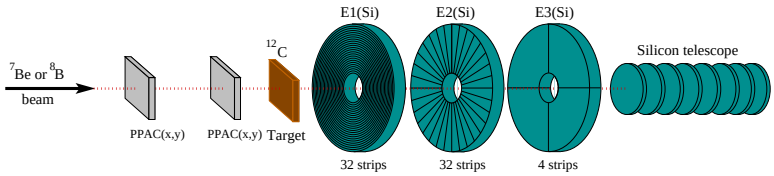

Figure 2: Schematic setup for the elastic scattering experiment.

Experimental investigations of the elastic scattering of exotic nuclei have allowed to obtain the important data on the structure of the interacting nuclei.

Neutron halo - ^{11}Li

RNB have been used to study the matter distribution and structure of neutron-rich nuclei by the elastic scattering. The aim of the first experiment was to advance the idea of a "nondestructive" study of ^{11}Li, by measuring its elastic scattering on a ^{28}Si target and to compare it to the elastic scattering of the stable nucleus ^{7}Li [A1].

The secondary beams of ^{7}Li and ^{11}Li with energies of 25.4 and 29 A.MeV, respectively, were produced by fragmentation of a primary beam ^{18}O (76 A.MeV) on a composite production target of 360 mg/cm^2 Be followed by 2900 mg/cm^2 of carbon. The LISE3 spectrometer [Ann92] was used to separate the secondary beam which was focused, subsequently, on the Si–detector serving as an active target. In this experiment the intensities of secondary beams 150 pps (^{11}Li) and 1000 pps(^{7}Li) were obtained. The scattered particles were detected by two annular thin Si–detectors and a terminal BGO–detector. The mass and the charge of scattered particles have been identified according to two-dimensional spectra obtained by combinations of their time of flight, energy losses in Si–transmission detectors and residual energy in the BGO–detector. The BGO–detector [A2] consisting of seven small BGO–crystals was built in the Czech Republic. Differencial cross sections of elastic scattering of ^{11}Li and ^{7}Li on a ^{28}Si target at angles $(5^o - 22^o)_{c.m.}$ were obtained.

The data were treated using a phenomenological analysis and by coupled channels calculations with a double-folding optical potential, with energy- and density-dependent effective interaction and realistic densities. The nuclear densities were constructed by standard Hartree-Fock (HF) calculation using Skyrme II (SkII) parametrization of the effective interaction [Vau72]. Spherical symmetry and occupation numbers determined by single-particle energies were assumed. Using CC calculations with the folding potential, a better description was achieved when the neutron halo of ^{11}Li was taken into account. In the analysis of both experiments considerable changes in optical potential parameters were necessary to reproduce the ^{11}Li elastic scattering data. In our experiment the use of a heavier target should, in principle, enhance the influence of inelastic processes such as break-up and Coulomb excitation of the projectile in the elastic channel, however, our results presented in Fig. 3 (left panel) have provided further support for the "neutron halo" hypothesis in ^{11}Li nucleus.

Neutron halo - ^{11}Be

One major characteristic of nuclear halo nuclei is the weak binding energy of the halo nucleon(s) and consequently the large breakup cross sections. As already known

since the early 1950s, the breakup of loosely bound nuclei is dominated by two major components: diffraction and/or Coulomb dissociation and absorption (or stripping). In the former case, the halo nucleus undergoes an excitation to the continuum due to the nuclear and electromagnetic mean field of the target. The weak binding leads to continuum admixture strongly affecting the ground state, and therefore this mechanism allows for a study of the halo-continuum response. In the later mechanism, the halo neutron is absorbed with the target and is removed from the incident beam.

Though considered in different theoretical approaches the two mechanisms have been rarely accessible experimentally, only their sum (total breakup cross section) being usually measured. However, the results presented in our work [A4] try to add some more to this picture. We used an integral method that allowed for a separate determination of the two contributions to the breakup cross section of ^{11}Be on silicon.

A ^{11}Be (43 A.MeV) secondary beam was produced at GANIL by fragmenting an ^{18}O (70 A.MeV) beam on a Be target. The fragmentation products were separated and formed by the doubly- achromatic spectrometer LISE. About 1000 pps of ^{11}Be hit a stack of 17 silicon detectors which formed a telescope serving as target, energy degrader, and detecting/identifying medium for the reaction products. In front of the telescope, an x-y position sensitive parallel plate avalanche counter (PPAC) controlled the centering and the size of the beam spot. The thickness of all the detectors were in

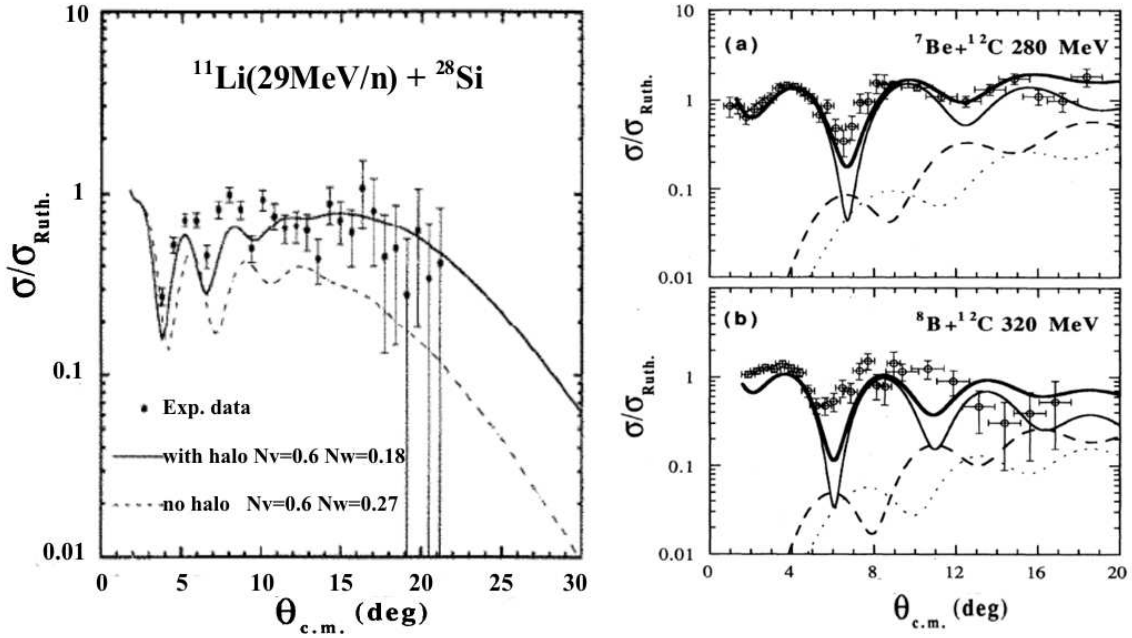

Figure 3: The elastic scattering of ^{11}Li + ^{28}Si(left), ^{7}Be and ^{8}B on ^{12}C (right).
Left – Angular distribution and CC calculation of ^{11}Li elastic scattering. The bare CC double-folding potential is calculated with DDM3Y and HF- SkII density for ^{28}Si and the halo density from ref. [Ber89] (solid line) and HF- SkII density (dashed line) for ^{11}Li. Right – the thin solid lines represent the elastic scattering, the dashed lines the CC calculation of the 2^+ state of ^{12}C. The dotted lines represent the DWBA calculation of the channel leading to the 3^- state, the incoherent sum - thick solid line.

total 7344 μm. Most of incident ^{11}Be ions have been stopped in the last two detectors of the telescope at about 6457 μm. If an incident ^{11}Be ion undergoes a breakup, the ^{10}Be, having a smaller energy, will be stopped earlier in the telescope than the incident ^{11}Be nucleus.

The study of the breakup and reaction cross sections of the ^{11}Be nuclei on the ^{28}Si target has been performed [A4] for the first time. The separate contributions of diffraction and absorption to the breakup cross section have been determined. The parallel momentum distributions for the ^{10}Be have been determined for the two breakup mechanisms. Charge changing cross sections have been measured for ^{11}Be and ^{10}Be as well as the two-neutron breakup cross section for ^{11}Be. Neutron angular distributions in coincidence with various reaction processes in the telescope have been obtained and interpreted in terms of phenomenological transverse momentum distributions. All the mentioned data taken in a single experiment provide new important information about the structure and breakup mechanism of the halo nucleus ^{11}Be in the energy range 20 - 40 A.MeV.

Nowadays, such a neutron halo structure has already been observed in a certain number of cases: ^{6}He,^{11}Li, ^{11}Be, ^{14}Be, ^{17}B and ^{19}B. There is no other physical system in Nature that has such a structure. The best known nuclei with halos of neutrons are ^{11}Be (1-neutron halo) and ^{6}He, ^{11}Li, and ^{14}Be (Borromean 2-neutrons halo). It was found that the nuclei with halos are between 20% and 30% larger than predicted by the well-established $A^{1/3}$ rule for stable nuclei. The distance between the halo and the core is distinctly larger than the range of the nuclear force. The valence nucleons thus have a very high probability of being very far from the core, which implies that they have a high probability of tunneling through the potential barrier (nuclear and centrifugal), and to penetrate into the classically forbidden regions. Furthermore, there are significant pairing effects between the neutrons of a Borromean system, even when both nucleons are in the classically forbidden space.

Proton halo - ^{8}B

To solve the question of the existence of a proton halo in ^{8}B is a difficult task. While the one-neutron halo in ^{11}Be and two-neutron halo in ^{11}Li are well established by experiment, the evidence for the proton halo is somewhat contradictory. Former experiments suggest either a large proton halo or a vanishing one. For example, Minamisono et al. [Min92] found an electric quadrupole moment much larger than the shell model would predict and this was interpreted as a strong evidence in the favor of proton halo. The experimental quadrupole moment could be explained using single particle wave functions (s.p.w.f.) which correspond to a matter density with a radius of 2.7 fm, i.e., much larger than the prediction of any selfconsistent calculation. It seems quite natural to expect such a halo for protons because of the charge symmetry of the nuclear force.

On the other hand, this experiment has to be compared with the older result of Tanihata et al. [Tan88] who obtained only a modest increase of the interaction cross section of ^{8}B as compared with ^{7}Be, the presumable core of ^{8}B. We should note that the Coulomb force among the protons besides the nuclear force may prevent the growth of the halo and push the protons inside the Coulomb barrier. As a result,

the proton halo may be less pronounced than the neutron halo even if it is formed. From an experimental point of view, it is difficult to detect the thin halo by interaction cross-section measurements because the method is mainly designed to observe matter distributions and therefore the effect due to the proton halo could be only a small fraction of the cross-section. Therefore our study [A3] of the ^{7}Be and ^{8}B nuclei predicted to be proton-halo nuclei was of a particular interest.

The secondary beams of ^{7}Be and ^{8}B with energies of 40 A.MeV were produced by fragmentation of a primary beam ^{13}C (60 A.MeV) on a Be target. The elastic scattering of ^{8}B and ^{7}Be on a ^{12}C target has been measured to compare a ^{8}B nucleus with its core ^{7}Be at the same velocity. The fragmentation products were subsequently separated using the LISE3 spectrometer as in the case of ^{11}Li. The secondary beam intensities were of about 1000 pps with purities better than 98%. Because of the large angular and energy spread of the secondary beams, X-Y position sensitive parallel-plate avalanche counters (PPAC) were used to determine the incident angle and position on the target for each incoming particle. Particles scattered on the target were detected by an assembly of three silicon strip detectors shown in Fig. 2. These detectors provided information on the scattering angle and the energy loss, which in combination with the residual energy provided by thick Si or BGO detectors [A2] were used for particle identification. However, energy resolution was not sufficient to distinguish fully between elastic and inelastic scattering and it resulted in the admixtures to pure elastic scattering. The used experimental method was carefully tested by ^{12}C + ^{12}C reaction.

Angular distributions measured in this experiment are shown in the right panel in Fig. 3. The experimental data are compared with theoretical calculations. The error bars indicated for the experimental data correspond to the statistical errors. The thin lines represent the elastic scattering, the dashed lines the CC calculation of the 2^{+} state of ^{12}C. The dotted lines represent the DWBA calculation of the channel leading to the 3^{-} state.

The double folding model associated with the effective interaction of JLM [JLM77] was chosen to construct the necessary elastic optical potentials and the form factors for inelastic scattering. The heavy ion optical potential U($\mathbf{R}$) has been constructed in the double folding model described in Sec.2.2 by eq. (6) for both real and imaginary parts as

$$U_F(\mathbf{R}) = N_V U_V(\mathbf{R}) + N_W U_W(\mathbf{R}), \tag{9}$$

where V,W represent real and imaginary parts of the optical potential. The diagonal part of the one-body densities for ^{7}Be and ^{8}B in the $\mathbf{r}$ - space has been obtained in a shell model calculation. The occupation probabilities were obtained by diagonalization of the Warburton-Brown interaction [WaB92] in first four major shells using the OXBASH code [OXB88].

The densities were calculated using the standard Hartree-Fock calculation with the Skyrme III parametrization and the occupation probabilities were taken from the shell model calculation. A DWBA and a coupled channels analysis with a semi-microscopic double folding optical potential have been applied on experimental angular distributions. The use of nuclear densities which exhibit a proton skin give a satisfactory angular distribution for both ^{7}Be and ^{8}B. The calculated one-proton removal cross-section also agrees well with the experimentally found cross-section.

Our experimental results and analysis [A3] suggest that the increase of the optical model reaction cross section is rather consistent with a normal dependence of the interaction radius R≈$A^{1/3}$. This can be due to the fact that the measured angular range for quasielastic scattering was too small to draw definite conclusions about the existence of the proton halo but does confirm the existence of the proton skin.

The semiclassical analysis of ^{8}B revealed a number of similarities with ^{11}Li resulting from a combined effects of a proton and/or neutron skin and the lower threshold for breakup. The stronger Coulomb interaction in ^{8}B confines the proton wave function in the nuclear interior and inhibits the development of a proton halo. The folding potentials generated by JLM microscopic effective interaction are much stronger for ^{8}B than for ^{7}Be in both real and imaginary parts.

Proton halo via reaction and breakup measurement

Simultaneously with the quasielastic scattering of ^{7}Be and ^{8}B [A3], the excitation function of the total ^{8}B +^{28}Si and the breakup ^{8}B +^{28}Si → ^{7}Be +X reaction cross sections have been measured for several energies in the range of $(10 - 40)$ A.MeV [A5, A6]. It has been believed that such a measurement, due to the very loosely bound nature of the projectile, would provide further information on the proton wave function. Complementary measurements of the reaction cross section of ^{7}Be on silicon have been performed in order to have a clear comparison of the core with the presumed halo nucleus.

In this experiment, the successively selected ^{8}B and ^{7}Be nuclei were directed on a stack which consisted of eleven Si thin detectors of various thicknesses and served as a target, degrader and detecting medium for reaction products. This device allowed to measure, except the reaction and breakup cross sections, also the parallel momentum distribution of ^{7}Be resulting from the ^{8}B breakup.

The selection of the reaction events is based on the observation that the energy deposit in the detector in which one of the reactions ^{7}Be +^{28}Si or ^{8}B +^{28}Si took place, is significantly different from that of the beam particles (non-reacting particles). Therefore a gate around the typical energy loss of the beam particles in a given detector is sufficient to determine the number of reaction events in that detector and to eliminate them from the flux impinging upon the next one(s).

On the other hand a breakup event is defined as one in which an incident ^{8}B ion propagates through the telescope up to a given depth, after which it turns into a ^{7}Be ion that will continue propagating up to the end of its range. However, in order to identify the ^{7}Be ion, it must penetrate through at least two detectors before reaching the end of its range.

The structure of ^{8}B is very important in connection with the astrophysical problem of solar neutrinos. The good agreement with the experimental data of the present optical model calculations give us confidence in the obtained wave function. Recently, Brown, Csótó, and Sherr [Bro96], deduced a theoretical relation between the absolute normalization of the proton valence density (i.e., the density value at r= 10 fm) and the astrophysical S_{17} factor for the ^{7}Be (p,γ) reaction. Using our density ρ (r=10 fm) and the spectroscopic factor calculated by Brown et al. one obtains S_{17}= 17.2 eV b. This is identical with the value obtained by Barker in an R-matrix approach [Bar95].

For the first time, the contribution to the breakup from the diffraction dissociation and absorption mechanisms were separately determined. We have deduced that the proton halo [A5, A6] is small compared to the neutron halo of ^{11}Be [A4] and ^{11}Li [A1] obtained in our experiments as an effect of Coulomb and centrifugal barrier confinement. Knowledge about ^{8}B nucleus is valuable both for astrophysical reasons and for clarifying the question of the existence of proton halo.

3.2 Matter distribution of neutron-rich nuclei

Reaction cross-sections measurement

The nucleon–nucleus potential has been studied extensively through elastic scattering measurements. Concerning the stable nuclei, a vast amount of experimental data for nucleon–nucleus elastic scattering was interpreted in the framework of phenomenological and microscopic potential models with the adjustment of none or only a few parameters, see for example [JLM77, Bec69, Sat79].

Reaction cross-sections are of fundamental interest in nuclear physics, since they provide a measurement of the size of the nucleus. They are an effective tool for revealing unusual features in nuclei such as extended neutron halo or skin [Tan85, Tan88, Suz95, Suz98]. At low energies, they also complement elastic scattering data to obtain an information on the nucleon–nucleus potential. When the radioactive beam facilities become available with higher intensities, the reaction cross-section measurements have been extended to neutron-rich nuclei close to the drip lines by using inverse kinematics (secondary beam incident on a proton target) which enables us to detect the reaction products in the narrow forward angle.

In our experiment [A7], the proton reaction cross-sections have been measured in inverse kinematics for stable and neutron-rich nuclei in the mass range A=4–32 on proton. The target was made of liquid hydrogen, and was used for the first time in this experiment. The measurements cover the intermediate energy region(35–75 A.MeV), while previous measurements, even for stable nuclei, existed only for energies lower than 48 MeV or higher than 100 MeV. The experimental values obtained in our work therefore fill this gap and are in good agreement with the general trend observed at lower and higher energies.

The first measurement of the reaction cross section of the halo nuclei ^{6}He and ^{11}Be on a proton target in this energy range was also carried out. The value measured for ^{6}He can be reproduced within the JLM approach with normalization factors very close to the standard values for the isoscalar part of the potential, provided that a normalization of 1.4 was applied to the isovector part, thus confirming the weakness of the isovector potential in the JLM approach [Pak01, Bau01, Die85]. It should be noted that a simultaneous analysis of elastic scattering and charge exchange angular distributions with the present reaction cross-section data for ^{6}He showed that the three data sets could be adequately reproduced with these normalization factors [Vis01]. A significant increase of the imaginary part of the potential was necessary in order to

reproduce the p + ^{11}Be reaction cross section.

Proton and neutron distribution in Mg isotopes

As we have mentioned in Sec. 1 some shell model calculations have demonstrated that for nuclei in the island of inversion the $2\hbar\omega$ configurations arising from the excitation of a pair of neutrons across the N = 20 shell gap to the fp orbits are more strongly bound than the $0\hbar\omega$ states and dominate intruder deformed ground-state configurations.

A related question is whether in these extreme conditions the deformation of proton and neutron distributions is identical or if a decoupling of the densities occurs. Identical deformations are predicted in the relativistic mean field and in the anti-symmetrized molecular model, whereas different deformations are obtained in the Hartree-Fock–Bogoliubov model (HFB) [Ter97] and in the standard shell model [Cau98]. Recent constrained HF calculations with a separable monopole interaction [Ste02] predict similar proton and neutron deformations.

To solve this question we have undertaken an experimental determination of the neutron and proton deformations of the ^{24,30,32}Mg nuclei at GANIL via inelastic scattering of these radioactive beams on ^{208}Pb and ^{12}C targets [A8]. The combination of these two measurements will disentangle the proton and neutron contributions, and lead to an assessment of the independent or mutual contributions of the neutrons and protons to the nuclear excitation.

The charged particle detection system consisted of three Si telescopes. The telescope Si3 was used to stop the secondary beam and to detect scattered particles at very forward angles. Two annular telescopes Si2 and Si1 covered the angular ranges larger than in earlier experiments [Mot95, Pri99], containing (2.1–4.5) and (4.5–10.0) degrees, respectively. The secondary beams could be clearly identified event-by-event in dE x TOF and dE x E spectra. For the detection of the γ-rays, we used two sets of 7 hexagonal NaI(Tl) detectors located at 90^o relative to the beam axis; 7 above and 7 below the target. The correction to the Doppler-shift and broadening due to the in-flight γ-ray emission of the scattered Mg nuclei was applied.

Finally, we have extracted the Coulomb and nuclear deformation lengths of ^{30,32}Mg by the inelastic excitation measurements of intermediate energy secondary beams on ^{208}Pb and ^{12}C targets. Both nuclei exhibit a similar value of $|\beta| \sim (0.5 - 0.6)$ of charge and mass deformations. The analysis within the collective model resulted in identical mass and charge deformations, giving no evidence for a large decoupling of neutron and proton deformations in this region.

4 Binding energy and Particle Stability

The binding energy represents one of a basic characteristic of the nuclear system. The the binding energy, i.e. the difference between the mass of a nucleus and the sum of the masses of its constituent free nucleons,reflects the forces of cohesion and provides direct information about the complex mechanisms that are responsible for the nuclear binding. The stable nuclei thus define the "valley of stability". All other nuclei convert to these nuclei by radioactive decay with lifetimes ranging from the smallest fraction of seconds to million of years. By adding either protons or neutrons, radioactive nuclei away from stability are formed, finally reaching the drip lines where the proton or the neutron separation energy becomes negative, and the last nucleon is no longer bound. Thus measuring the binding energy is important since it allows us to locate the drip lines experimentally that provides an excellent means of testing our nuclear models, and enables to recognize where the shell closure occurs far from stability. Very neutron-rich nuclei also offer the opportunity to study pairing phenomena in systems with strong density variations.

The experimental determination of the neutron drip line is very important for the understanding of nuclear stability in extreme values of isospin. During the last decade, our knowledge has been considerably extended concerning the stability of extremely neutron-rich isotopes, renewed effort to search for new isotopes has been encouraged and many significant achievements have been obtained in the field.

The particle stability of nuclei far from stability has been an issue of much interest in nuclear structure ever since the neutron rich Na and Mg nuclei around N = 20 were found to be more bound than predicted by a spherical closed-shell prescription. Shell model calculations [Pov87, War90, Fuk92, Pov94, Cau98] have demonstrated that for Z = 10–12 and N = 19–22, the $2\hbar\omega$ configurations arising from the excitation of a pair of neutrons across the N = 20 shell gap to the fp orbits are more strongly bound than the $0\hbar\omega$ states and dominate ground-state configurations, producing the "island of inversion". A related question is whether in these extreme conditions the "standard" neutron magic numbers can survive the deformation of proton and neutron distributions.

4.1 Particle stability of doubly-magic nuclei

During more than 30 years a number of experiments [Ste88, Dlo92] have been carried out to search for the doubly-magic ^{10}He nucleus which, if bound, would possess the highest N/Z ratio among all known nuclei. The experiments led to the conclusion supported by fragmentation studies that ^{10}He is probably unbound.

In 1994 Korsheninnikov et al. [Kor94] investigated the ^{11}Li fragmentation using an invariant mass measurement and was successful in the observation of a peak in the ^{8}He+n+n coincidences which could be explained by the ^{10}He resonance at the energy 1.2 ± 0.3 MeV above the ^{8}He+n+n threshold. The energy of ^{10}He was found to be close to the predictions given by the shell model estimation (1.18 MeV).

At the same time, Ostrowski et al. [Ost94] measured the mass and two excited states of ^{10}He with the ^{10}Be(^{14}C,^{14}O)^{10}He reaction at E=24 A.MeV. The ground state

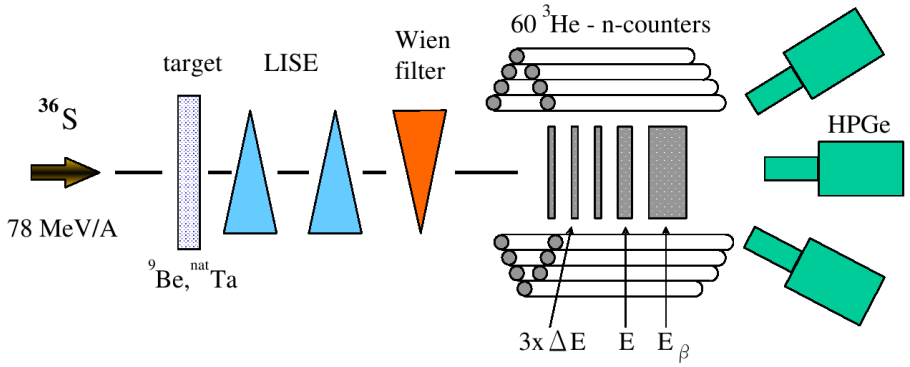

Figure 4: Setup for search for doubly-magic nucleus ^{28}O.

resonance was found at mass excess of 48.81(7)MeV. It is 1.07(7)MeV above the ^{8}He +2n threshold. Two excited states were observed at 3.24(20) and 6.80(7)MeV with a preliminary spin assignment 2^+ and 3^-, respectively. From the existence of the relatively low-lying 2^+ state, the authors concluded, that the shell closure probably does not manifest itself at the neutron number N=8, but is shifted to N=10. There are indications in neighbouring nuclei, that the ν $1s_{1/2}$ orbit moves down close to the ν $0p_{1/2}$ orbit.

Therefore, in our experiment on the LISE3 spectrometer at GANIL, we have used the fragmentation of the neutron-rich projectile ^{36}S to synthesize light very neutron-rich nuclei in the vicinity of the doubly-magic nucleus ^{28}O (Z=8, N=20), in order to determine the particle stability and to study the properties of these nuclei [A9]. The particle stability of ^{26}O has been predicted by many theoretical models, even though the particle instability of ^{25,26}O has clearly been shown in two experiments [Fau96, Gui90]. On the other hand, the ^{28}O nucleus was predicted to be particle unbound despite of its double magicity.

The fragmentation of a ^{36}S^{16+}(78.1 A.MeV) beam on a ^{nat}Ta (643 μm) target was used in the search for heavy oxygens. After passing through the target, the reaction products were focused and separated by a system of quadrupole lenses, two dipole magnets operated in achromatic mode (with rigidity 4.3 and 3.2 Tm) and Wien filter. Products overcoming a full flight distance of 42 m, entered the detection chamber (see Fig.4.) were identified unambiguously by the time-of-flight method, the energy loss and the total kinetic energy TKE, measured by five planar surface barrier Si and Si(Li) detectors of different thickness mounted in a vacuum chamber at the achromatic focal point of LISE3.

In our experiment, no events corresponding to ^{26}O and ^{28}O were observed as one can see from the identification matrix accumulated during 53 hours of measurement shown in Fig.5. Moreover, no events corresponding to the odd oxygen isotopes ^{25,27}O, to ^{24,25}N or to ^{23}C were present. According to the experimental dependence of the measured yield of light nuclei with N=20 on the number of protons removed from ^{36}S also shown in Fig.5, we expected to observe about 11 events of ^{28}O. Upper limits of the cross sections for the formation of the oxygen isotopes were estimated to be 0.7 pb and 0.2 pb for ^{26}O and ^{28}O, respectively. Thus the unbound character of both ^{26}O and ^{28}O nuclei was firmly established [A9]. Therefore, till now, the heaviest experimentally

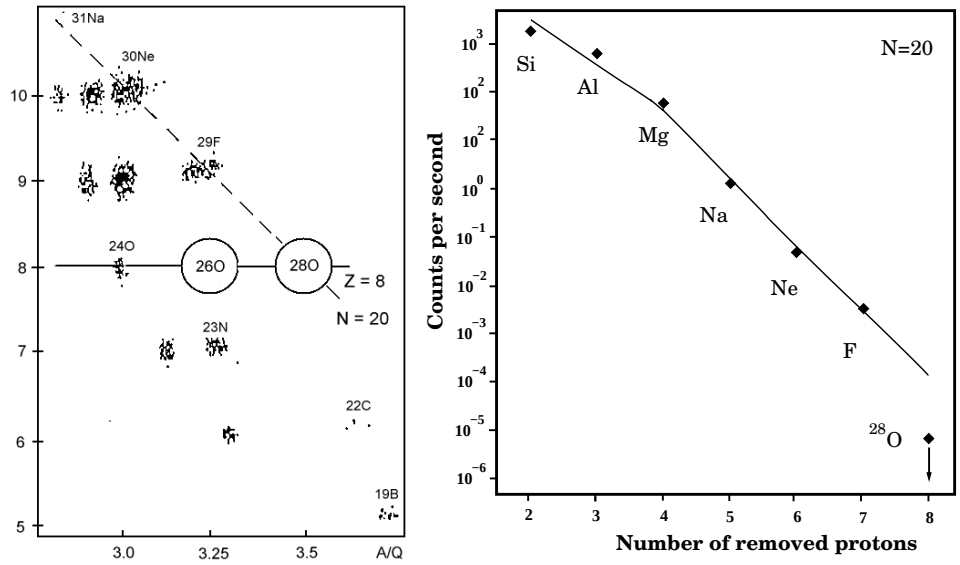

Figure 5: Two-dimensional identification plot A/Q versus Z (left); no counts have been observed for ^{24,25}N, ^{25,26,27,28}O. Yields of N=20 isotones measured in experiment (right); the point with arrow for ^{28}O corresponds to the upper limit of one detected event.

found oxygen isotope remains to be the ^{24}O nucleus.

Our finding that ^{28}O is unbound [A9] fairly supports the idea that the onset of the deformation found in the Ne-Al region is due to the breaking of the magicity of the N=20 shell closure in ^{28}O nucleus. The neutron drip line up to fluorine has also been investigated by Sakurai et al. [Sak99] by the projectile fragmentation of a ^{40}Ar(94.1 A.MeV) beam at the fragment separator RIPS at RIKEN. A new neutron-rich isotope ^{31}F has been observed for the first time while the firm confirmation of the particle instability of ^{24,25}N and ^{25,26,27,28}O has been obtained. In both experiments [A9,Sak99] the calculated and observed yields of isotopes have been in good agreement and have provided a strong evidence for the particle instability of ^{23,24}C, ^{24,25}N, ^{25,26,27,28}O and ^{30}F.

Concerning the instability of ^{24,25}N, mass formula predictions are in agreement with both experimental results. On the other hand, the location of the drip line for oxygen and fluorine are poorly predicted by the mass formulae, most of which favour ^{26}O and ^{29}F as the heaviest isotopes.

4.2 Particle stability near the drip line

The particle stability of ^{31}F gives strong evidence of the onset of deformation in the region. Therefore, one may expect that the drip line for the fluorine-magnesium elements could move far beyond the presently known boundaries.

In our work [A11], we present the results of our attempt to determine the neutron drip line for the Ne-Mg isotopes. In particular, our experiment was dedicated to the direct observation of the ^{34}Ne, ^{37}Na and ^{40}Mg nuclei. The beam of ^{48}Ca(59.8 A.MeV) with mean intensity of about 150 pnA was fragmented on a Ta(160 μm)target. The

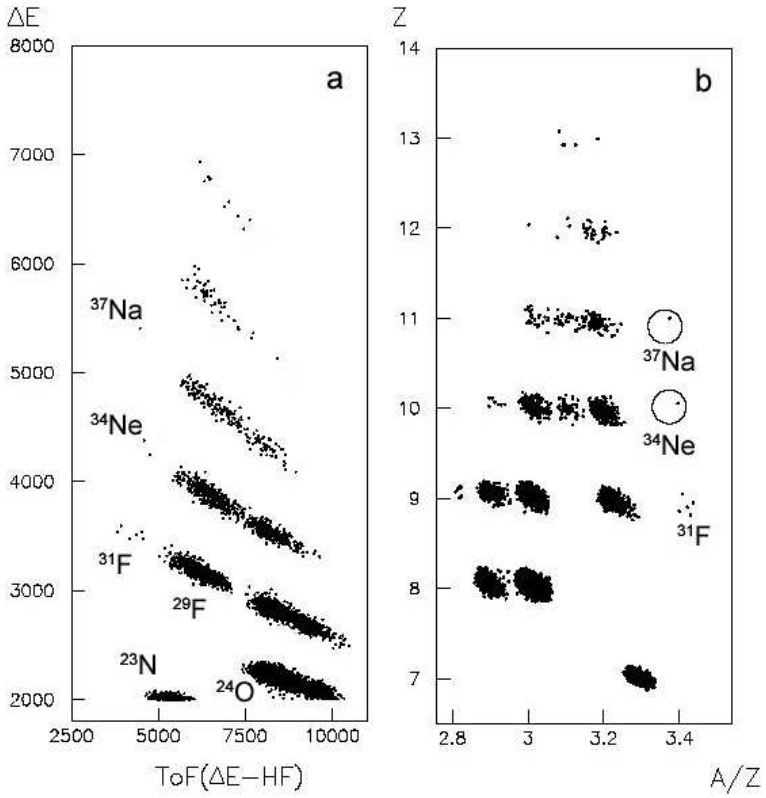

Figure 6: (a) Energy loss versus TOF identification matrix. (b) Two-dimensional Z versus A/Z plot. The new isotopes ^{34}Ne and ^{37}Na are clearly visible. No events associated with ^{33}Ne, ^{36}Na and ^{40}Mg have been observed.

experiment benefited from a recent upgrade of the LISE spectrometer. A total increase of a factor of 10 in the production rate of the drip line nuclei has been achieved. In addition to the standard identification method of the fragments via time-of-flight (TOF), energy loss (dE) and total kinetic energy (TKE), a multiwire proportional detector was placed in the dispersive plane of the LISE 2000 spectrometer. The detector allowed to measure the magnetic rigidity of each fragment via its position in the focal plane, improving the mass-to-charge resolution (A/Q). The selected fragments were implanted in a telescope consisting of seven silicon detectors for the identification of the fragments. In the data analysis, the fully stripped fragments were selected by putting gates on the total kinetic energy measured with the Si telescope.

The result of the particle identification based only on dE, TOF and TKE is shown in Fig. 6(a), where the energy loss measured in the first detector of the telescope is plotted versus TOF between the response of dE silicon detector and the cyclotron radio-frequency, HF. The new isotopes ^{34}Ne (two events) and ^{37}Na (one event) which have also been unambiguously identified using the calculated value of A/Z are clearly visible. This value was obtained from the TOF and from Bρ, measured by means of the multiwire detector.The discovery of ^{31}F [Sak99] was also confirmed. Two-dimensional A/Z versus Z plot is shown in Fig. 6(b). The presence of the events corresponding to ^{34}Ne and ^{37}Na confirms that these nuclei are bound. One event of ^{34}Ne in Fig. 6(b) is absent due to the fact that the efficiency of the multiwire detector for light fragments is

only 80%. No events which could be attributed to ^{33}Ne, ^{36}Na and ^{40}Mg were observed.

The most interesting nuclide in this region is ^{40}Mg. No counts attributed to ^{40}Mg have been observed in the present experiment. We estimated the upper limit for the production cross section of ^{40}Mg to be less than 0.06 pb. Due to the limited statistics the present experiment does not allow us to draw a definite conclusion on the instability of ^{40}Mg. The production cross sections of ^{34}Ne and ^{37}Na were estimated to be about 0.17 ± 0.12 pb and 0.06 ± 0.06 pb, respectively. The cross section of ^{31}F is estimated to be about 0.7 pb. According to our results, the neutron drip line extends beyond N=20 and reaches N=24 for neon and even N=26 for sodium isotopes most probably as a consequence of the mixing of the $d_{3/2}$ and $f_{7/2}$ states.

We note that during experiment the oxygen, fluorine and neon isotopes were implanted in a Si telescope and after delayed β-decay [A10] their γ spectra were detected by four HPGe detectors. The analysis of this part [A12] of our experiment will be presented in Sec. 6.1.

5 Nuclear Masses and Magic Numbers

5.1 Direct mass measurement

To explain the instability of the ^{28}O nucleus and the onset of deformation at the island of inversion an experiment on mass measurement was undertaken at GANIL. Nuclear masses are usually measured either "indirectly" using a reaction or radioactive decay and energy conservation or "directly" through frequency or time-of-flight measurements. While the former methods involve a knowledge of the details of the relevant reaction or decay, the latter involve the calibration of the corresponding frequency or time-of-flight scale. Since the question of particle stability is directly related to the masses and nuclear binding energies, which are very sensitive to the existence of shells and may provide clear signatures of shell closures [Mit97] the mass measurement of nuclei from Ne to Ar can bring some clarifications concerning the behaviour of magic numbers far from stability.

The nuclei of interest were produced by the fragmentation of a ^{48}Ca(60 A.MeV) beam on a Ta target located in the SISSI device of the accelerator complex at GANIL. The mass was deduced from the relation $B\rho = \gamma m_0 v/q$ where $B\rho$ was the magnetic rigidity of a particle of a rest mass m_0, charge q and velocity v and γ was the Lorentz factor. This technique has already been used at GANIL to measure the masses of a large number of neutron-rich nuclei [Gil87]. The 82 m long flight path between a start detector located near the production target and a stop detector at the final focal plane of the high resolution spectrometer SPEG facilitated the time-of-flight measurement. The magnetic rigidity was measured in the dispersive section of the SPEG spectrometer using a position sensitive detector. Unambiguous particle identification was provided by a four-element silicon detector telescope. Depending on the statistics, a final precision in the mass excess ranging from 100 keV (for thousands of events) to 1 MeV (for tens of events) was obtained.

We have measured 31 masses of neutron-rich nuclei in the range A=29–47 [A13]. The precision of 19 masses has been significantly improved (with the uncertainty bet-

ter than 1 MeV) and 12 masses were measured for the first time. The experimental shell corrections and the comparison of the measured mass excess with models show a weakening of the N=28 shell closure.

5.2 Two-neutron separation energy

The two-neutron separation energies S_{2n} derived from the measured masses are displayed in Fig. 7. Such systematics are of a particular interest as the S_{2n} values correspond to a "derivative" of the mass surface. Our new data [A13] are presented with error bars while the others, except the encircled data, are taken from Audi and Wapstra [Aud97].

A behaviour typical of the filling of shells can be seen from the characteristics corresponding to the Ca, K and Ar isotopes. The two shell closures at N=20 and N=28 are evidenced by the corresponding sharp decrease of the S_{2n} value when two neutrons are added after crossing magic numbers (N=20 and 28). After this sharp drop at the point N_{dp} (corresponding to N_{shell}+2) the S_{2n}values step-down only slowly as the filling of the next shell starts to influence S_{2n}.

However, such simple behaviour as presented for N=28 cannot be seen in other elements. As it has been already pointed out in our work [A12] the situation for Cl, S and P isotopes exhibit a pronounced change of slope around N=26. The observed trends are well reproduced by large scale SM calculations undertaken within the $sd-fp$ model space [Ret97]. A similar agreement was obtained in our relativistic mean field, RMF, calculations except for the odd-even staggering which was not perfectly reproduced and may indicate a need to fine tune the pairing force.

The discontinuity observed at N=26 in Fig. 7 appears also as a sufficiently large gap at N=26 for Z=15, 16 and 17 on the plot of S_{2n} versus Z in Fig. 9. This discontinuity can now be understood in a simple Nilsson picture. For a prolate deformation of $\beta_2 \sim$

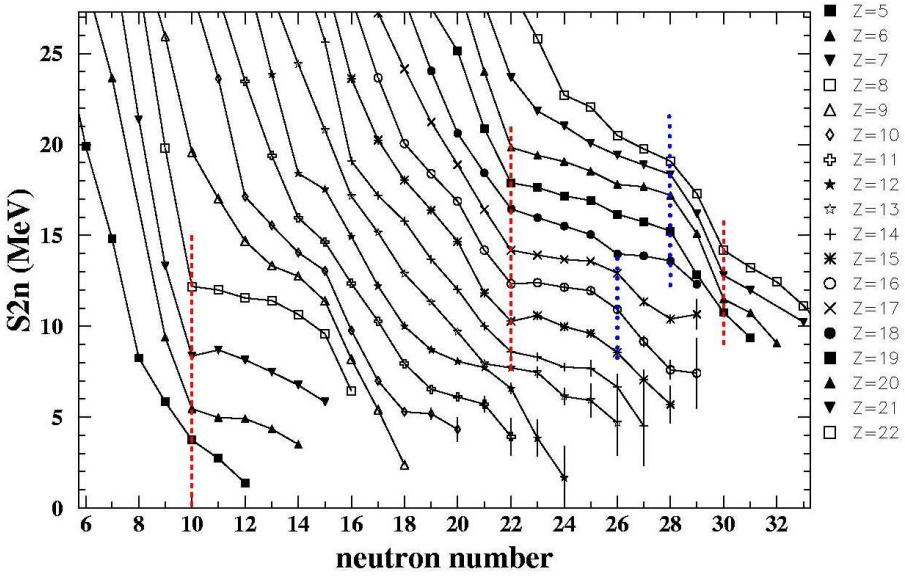

Figure 7: Two-neutron separation energy S_{2n} versus N.

0.2, a large gap appears between the lowest three orbits and the fourth orbit arising from the $0f_{7/2}$ and higher orbits. Oblate deformations would not be compatible with these observations. Consequentally, a pseudo-shell closure can be considered to appear at N=26.

However, the situation at N=20 shell closure looks much more regularly. The sharp drop at N_{dp}=22, shown by the dashed vertical line and corresponding to the shell N_{sh}=20 is clearly visible through all the Si-Ca region. We should note that if we go to lower Z (the Al-Na region) the drop point N_{dp} seems to move towards lower N.

As it can be seen in Fig. 7 interesting new results have also been obtained, for the Ne to Al isotopes. In particular, the steep decrease of the S_{2n} for ^{35,36}Mg suggests that the Mg isotopes may become unbound at much lower neutron number than the predicted value of N$\geq$ 28. The confirmation of this fact could come from the gap opening at very low S_{2n} separation energies at N=22 for 12$\geq$Z$\geq$9 in Figs. 7-9, and also from our search for stability of semi-magic ^{40}Mg [A11] described in Sec. 4.2 which has pointed out the very low probability of the existence of this isotope. However, further experimental and theoretical work is required to confirm this conjecture.

5.3 Magic numbers

The complex situation in the O-Al region mentioned above was also the reason why we made an attempt to clarify the behaviour of two-neutron separation energies in this region. We used the fact that several particle stable nuclei [A9, Sak99, Sak96] were found to exist in this region, however, their masses are not known yet. Nevertheless, their S_{2n} values must be positive and therefore, we included the "expected" S_{2n} values of the heaviest particle stable isotopes ^{23}N, ^{22}C, ^{29,31}F and ^{31,32}Ne to the plot (circles). The "expected" S_{2n} values for ^{29,31}F and ^{31,32}Ne point out the region where they probably have to be located due to their experimentally found particle stability (positive S_{2n} values) in Fig. 8. Their values have been tentatively estimated as a half of the S_{2n} value of the preceding particle stable isotope to ensure the most probable decrease of S_{2n} values.

The inclusion of the S_{2n} values for ^{29}F and ^{31}F was most important, because this allowed us to observe the sharp drop of S_{2n} value for ^{27}F (N_{dp}=18) followed by a moderate decrease of values for ^{29}F and ^{31}F. Such behaviour is very similar to the sharp drop near N_{dp}=22 (for N=20 shell closure in the Si-Ar region) just giving a very clear evidence of the existence of the new shell closure at N=16 [A14, A15]. A similar behaviour confirming the N=16 shell closure can be seen at the neon isotopes that exhibit a moderate decrease of S_{2n} values for ^{29}Ne,^{30}Ne and ^{31}Ne. The S_{2n} values at the drop points N_{dp}=10, 18, 22 and 30 corresponding to shell closures at N=8, 16, 20 and 28, respectively, are shown by vertical dotted (red) lines in Fig. 8.

Another evidence for the existence of the new shell N=16 appears from the behaviour of the "expected" S_{2n} values of the heaviest particle stable isotopes ^{23}N and ^{22}C have been placed in the plot to follow the trend seen in oxygen isotopes with N$\geq$ 14. The position of values are not crucial for determination of the shell closure at N=16, only the fact already observed in our experiment [A9] that particle stable isotopes heavier than ^{23}N and ^{22}C do not exist is important.

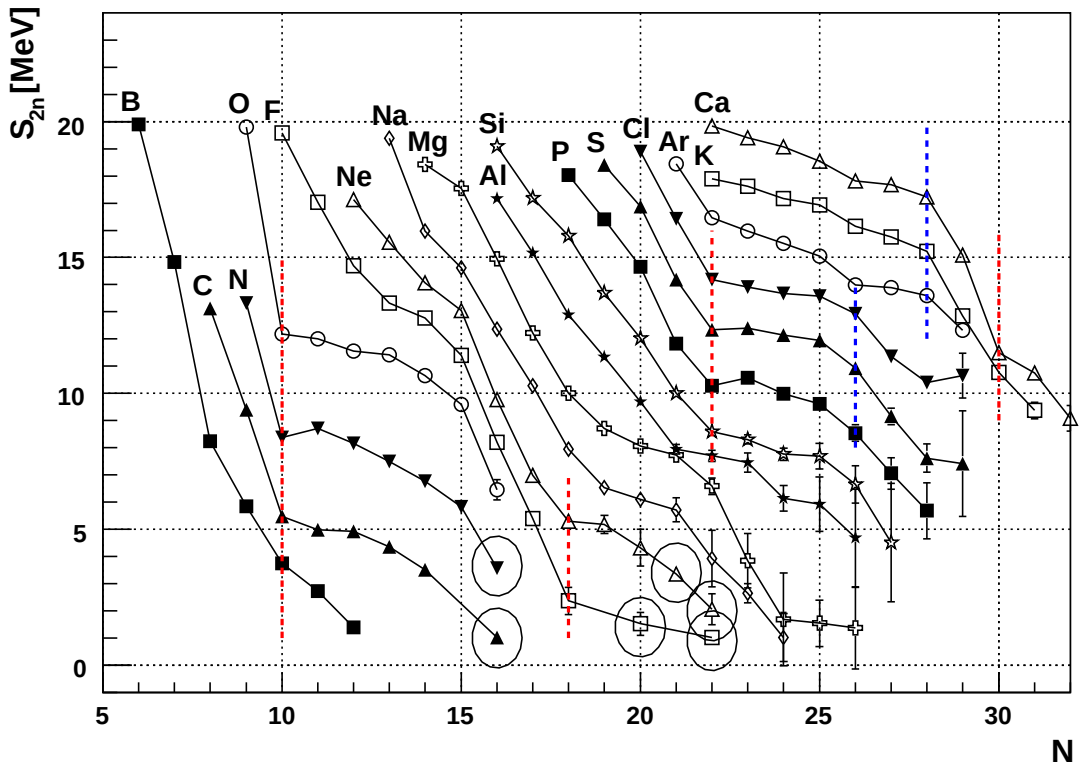

Figure 8: Two-neutron separation energy S_{2n} versus N – the drop points are visualized by vertical dotted red lines

It should be noted that the evidence of a new magic number N=16 follows also from Fig. 9 where the S_{2n} values are plotted versus an atomic number Z. The position of various possible shells or pseudo-shells are also shown in the figure. The shells N=20 and 28 appearing in Fig. 8 are very clearly seen as large gaps in Fig. 9. However, the gap corresponding to N=20 is narrowing when we go to lower Z, till finally, it completely disappears at Z=13 to emerge as the new N=16 gap at Z=10. This new gap governs over most of light Z neutron-rich nuclei and extends from carbon to neon. As one can see only the even-N nuclei are plotted on the right panel. However, the detailed plot of odd-N nuclei versus Z presented in our ref. [A16] shows that a similar role as N=16 for even-N nuclei is played by a gap N=15 for odd-N nuclei.

So we can state that a new shell closure at N=16 has appeared in neutron-rich nuclei for Z$\leq$10 between the $1s_{1/2}$ and $0d_{3/2}$ orbits in a good agreement with Monte Carlo shell model calculations of Utsuno [Uts99] and Otsuka [Ots01] and also with recently published work of Ozawa et al. [Oza00]. However, in this work an information on the magicity of N=16 is not so convincing since one-neutron separation energies S_{1n} were plotted only for odd-N nuclei and the measurement of the interaction cross section of radioactive beams σ_I is completely confusing.

The detailed inspection of neutron-rich region presented in Fig. 9 shows the interplay between gaps at N=8 and N=6. The gap corresponding to the N=8 is very large for Z$\geq$6, however, it is narrowing for lower Z in such a way that for Z=3 and 4 the new gap

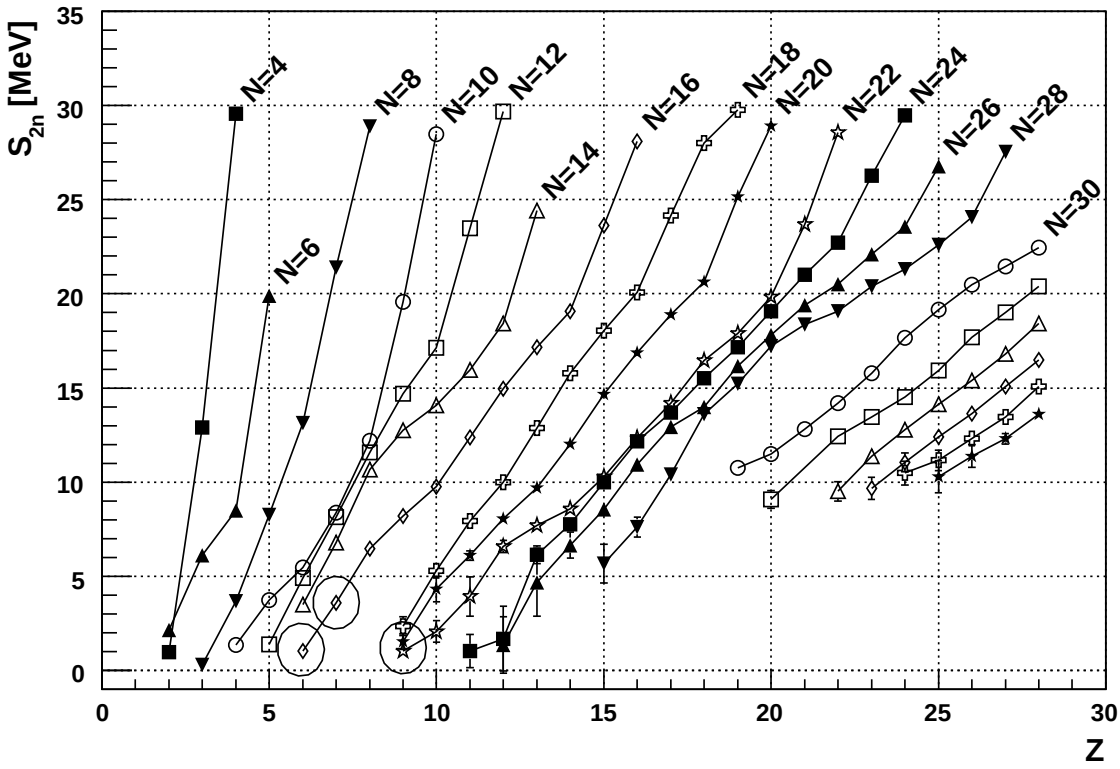

Figure 9: Two-neutron separation energy S_{2n} versus Z

at N=6 prevails. Thus this behaviour of separation energies confirms our assumption that when ^{10}He is unbound then there should be another magic number for neutron-rich nuclei. Due to the large gap at N=6, we can await that N=6 can be the new magic number. This fact gives the evidence that instead of formerly predicted ^{10}He the really existing doubly-magic nucleus is ^{8}He. So another new shell closure has also appeared in neutron-rich nuclei at N=6 due to the push of the $0p_{1/2}$ orbit to higher energies.

In our experiment, a new isomeric state in ^{43}S has been observed. The ground state has no longer a standard spherical configuration and spin $7/2^-$, but a deformed configuration and spin $3/2^-$. The existence of such an isomer can be explained in a shell model picture by inversion of a spherical to a deformed configuration. Coexistence and inversion of spherical and deformed configurations would thus be the origin of the observed behaviour.

In order to establish further evidence of existence of the N=16 shell we have tried to analyze the form of the two neutron separation energy dependence on neutron number near the shell closures [A18]. Since the slope of S_{2n} for the nuclei located in the valley of stability changes very drastically, mainly at the drop points (N_{sh}+2) corresponding to the shell closures at N_{sh}=8 and 20, we decided to use the angle between the slope for isotopes with N<(N_{sh}+2) and the slope corresponding to N>(N_{sh}+2), i.e. before the shell closure and during the filling of the next shell, to identify the neutron magic numbers. In the first step we applied this procedure only to nuclei lying near the valley of stability.

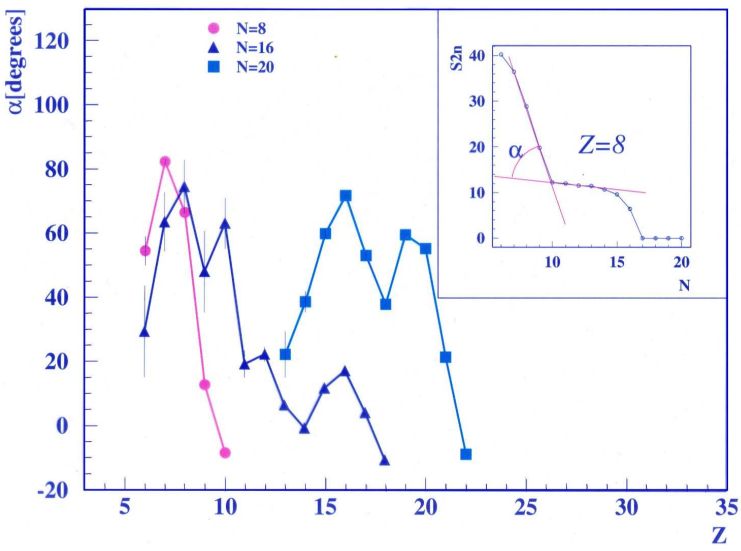

Figure 10: Experimental data of the angle α obtained for nuclei near the valley of stability show the region of Z where magic neutron numbers N=8, 16 and 20 are active; N_{sh}=8 (circles), N_{sh}=16 (triangles) N_{sh}=20 (squares). In the inset the angle α in two-neutron separation energy vs. neutron number plot at the drop point N_{sh}+2 (corresponding to N_{sh}=8) is shown.

The dependence of the angle α (shown in the inset) on the proton number for N_{sh}=8 and N_{sh}=20 is shown in Fig. 10 as circles and squares, respectively. Two peaks corresponding to nuclei embedded in the valley of stability and close to the magic neutron numbers N=8 and 20 are clearly seen and confirm the possibility to identify the magic numbers using changes of the S_{2n} slope. It should be noted that α values below 20 degrees are not significant. The nuclei near the neutron drip line and displayed in Fig. 10 as triangles possess also a relatively high α-value obtained for the shell closures at N=16. Thus the neutron N=16 magicity in the region from carbon up to neon is confirmed.

5.4 Microscopic energy

Another direct way to observe shell effects in neutron-rich nuclei is to compare their experimental and predicted mass values [A16, A17]. The difference between the experimental mass excess, ΔM_{exp}, and the result of calculated masses can be plotted versus the neutron number for different elements. We took the mass excess predicted by Finite Range Liquid Droplet model FRLD [Mol95] as ΔM^{FRLD}. The existence of the N=16 gap should manifest itself as a minimum of the shell correction, ΔM, which reads

$$\Delta M = \Delta M_{exp} - \Delta M^{FRLD}. \tag{10}$$

The comparison of the experimental mass excess and its theoretical predictions is plotted in Fig. 11. Well pronounced minima in the shell corrections appear at N=16 (or 15) for nuclei from oxygen up to aluminium. One might observe an increase of this difference as the neutron excess increases to Al isotopes. One can observed a minimum at

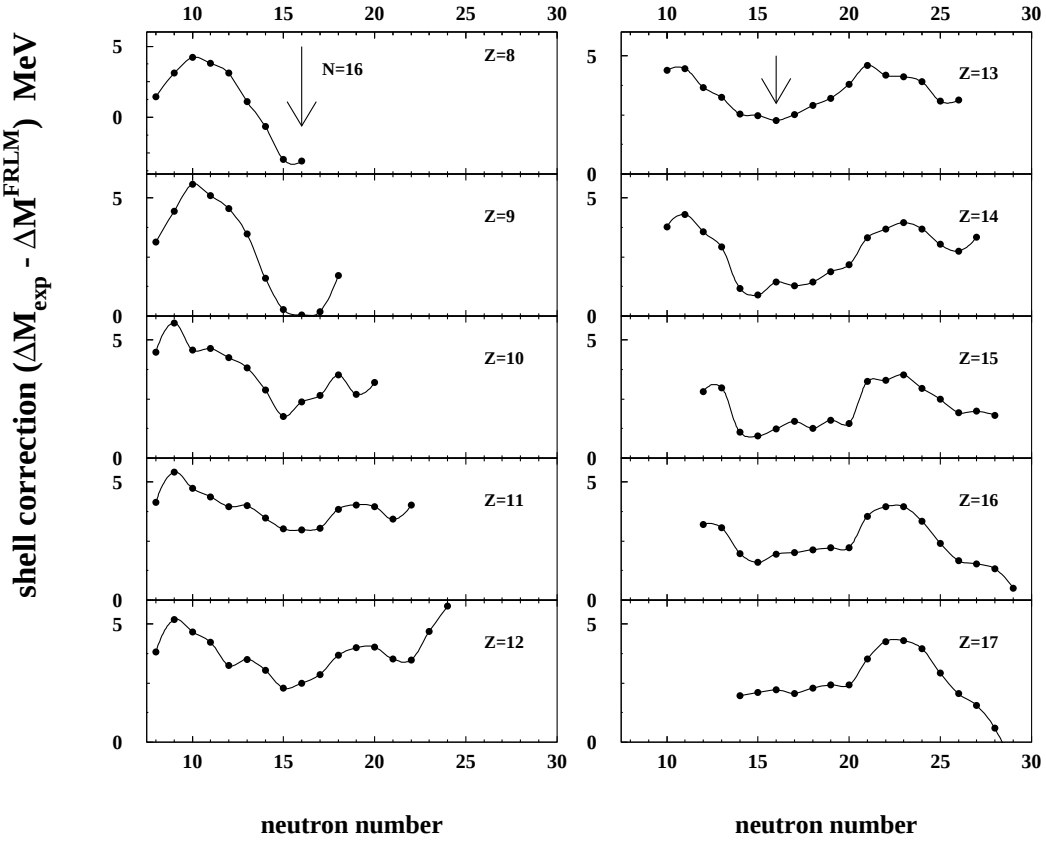

Figure 11: Dependence of the ΔM for the proton numbers Z=8–17.

N=20 only for P and higher isotopes. This gives further important evidence for the existence of the new shell closure at N=16 in neutron-rich nuclei in the oxygen-aluminium region.

6 Gamma Spectroscopy of Neutron-rich Nuclei

To the basic nuclear properties, except mass, binding and separation energies belong also the nuclear shapes and the structure of atomic nuclei. Very useful way how the precise deformation of nucleus can be determined is to measure the γ-rays emitted by excited nuclei and compare their energies and relative intensities. Nuclei possessing neutron/proton ratios radically different from those of the stable isotopes exhibit unexpected phenomena which have revolutionized our understanding of nuclear physics. Properties such as neutron halos and the modification of shell closures are predicted for a wide range of extremely neutron-rich nuclei, but it is only for the lightest elements that nuclei at the neutron drip line can presently be accessed experimentally. Although the neutron drip line has probably been delimited for elements below fluorine and the atomic masses of many of these nuclei measured [Orr91] comparatively little is known about their decay characteristics or spectroscopy [End90]. Such measurements can probe important details of the underlying microscopic structures which give rise to the novel phenomena.

6.1 Beta-delayed γ-ray spectroscopy

The probability of β-decay to states in the daughter nucleus provides an information on the degree of overlap between the neutron and proton states in the parent and daughter nucleus. When the radioactive decay populates excited states of the daughter nucleus, observation of the radiation associated with their de-excitation yields invaluable spectroscopic information on the energies and characteristics of low-lying excited states.

We used the experiment on the ^{28}O particle stability [A9] described in Sec. 4.1 to measure the β-delayed γ-rays of neutron-rich nuclei in this region. The spectrum of the β-delayed γ-rays enables one to characterize the structure of the states of the daughter nucleus, concerning its deformation or the arrangement of its particles.

The energy spectra of excited levels of certain nuclei reasonably close to the stability have been measured using transfer reactions [Orr89], but rapidly diminishing cross sections limit the range of nuclei which are amenable to study using this approach. A complementary tool is the β-delayed γ-ray spectroscopy, which can probe a different subset of excited states and, provided the decay schemes can be interpreted, can measure level energies with a greater precision. In principle β-decay measurements can be applied to nuclei right up to the neutron drip line, as long as the nuclei of interest can be cleanly and efficiently separated and their radioactivity measured with high sensitivity.

In our work [A12], β-delayed γ-ray and neutron emission has been studied for the first time in a range of neutron-rich nuclei extending out to the A/Z=3 nuclides $^{24}_{8}$O, $^{27}_{9}$F, and $^{30}_{10}$Ne. The first β-delayed γ-ray measurements for ^{25,26}F, and ^{26,28,29}Ne are also presented (see Fig. 12) and the half-lives and neutron emission probabilities measured in our work for all these nuclides are summarized [A10]. Possible level schemes deduced from the γ-ray spectra are compared with the results of transfer reaction studies and shell model calculations. These result are, partially, presented with other bulk of data obtained from in-beam spectroscopy in Sec. 6.2.

6.2 In-beam γ-ray spectroscopy

To obtain the information on shell closures atomic masses of many of neutron-rich nuclei up to Ar have been measured, and the neutron drip line has probably been delimited for elements below fluorine. However, such information can also be obtain from

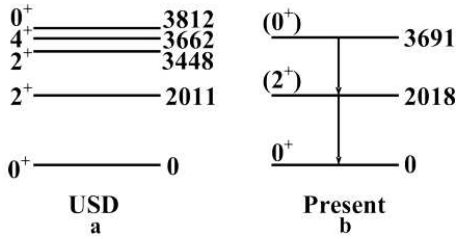

Figure 12: Energy levels of ^{26}Ne: **a)** nuclear levels predicted using the shell model with the USD interaction [Wil84]; **b)** the partial level scheme deduced in ref. [A12]. The excitation energies of the levels and γ -ray transition energies are given to the nearest keV. The spin and parity values in parentheses indicate tentative assignments.

the study of radioactive decay characteristics or spectroscopy of these nuclei. Since the spectroscopic measurements can reveal details of the underlying microscopic structures, and determine the shape of the nuclei under study, we have performed the first measurement at GANIL [Lop99, A17, A19] of the so called "in-beam γ-ray spectroscopy". Thus a very elegant way to identify shell effects experimentally is to measure the nuclear collectivity. In particular, Coulomb excitation combined with the measurement of the deexcitation γ-rays, gives access to the energy of the first 2^+ excited state and the associated B(E2) transition rate in even-even nuclei. When such data are systematically analysed as a function of proton and neutron numbers, the magic gaps are signalled by peaks in the 2^+ energies associated with corresponding dips in the B(E2) values. Deviations from the corresponding trends observed in stable nuclei may be used as indications of changes in the shell structure of nuclei. Again, the quantitative analysis must involve careful consideration of possible shape coexistence effects and/or effects associated with the proton-neutron composition of low-lying collective vibrational states, keeping in mind that only the proton component is responsible for the electromagnetic de-excitation. Additional information on relative intensities and the $E(4^+)/E(2^+)$ ratio is also highly desirable.

In order to obtain information on the structure of neutron rich nuclei in the proton-*sd* shell region, in-beam γ-ray spectroscopy using the projectile fragmentation reactions has been used. In these experiments shown schematically in Fig. 13 a large number of exotic nuclei have been produced and excited by fragmentation of neutron-rich projectiles (such as ^{36}S and ^{48}Ca) on a thin Be(2.77 mg/cm^2)target.

Experiments were based on measurement of coincidences between the projectile like fragments and their prompt γ-decay detected by γ-detector array. The Crystal ball consisting of 74 BaF_2 detectors shown in Fig. 14 has been used to detect γ-rays in all in-beam experiments. Detectors have been placed at a mean distance of 30 cm from the target covering nearly 4π. The relatively high velocity of the produced projectile fragments ($v/c \approx 0.35$) necessitates a proper Doppler correction of the detected γ-rays energies. The total photo-peak efficiency of the BaF_2 array was found to be 30% at 1.3 MeV with an average full width at half maximum of 12% after Doppler correction. The energy threshold of the BaF_2 detectors has been adjusted to a minimum value in order to allow the detection of low energy γ-rays down to 100 keV. Six Ge segmented

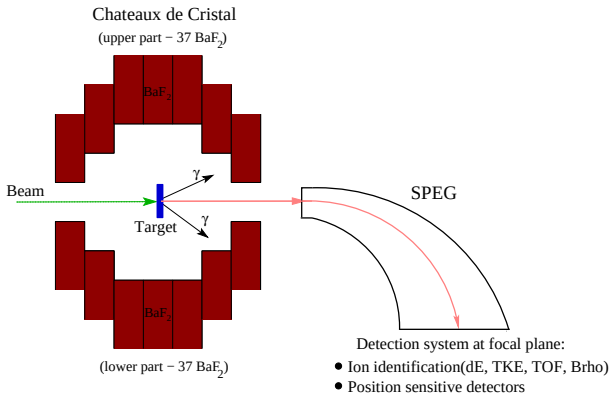

Figure 13: Experimental setup of in-beam spectroscopy measurement

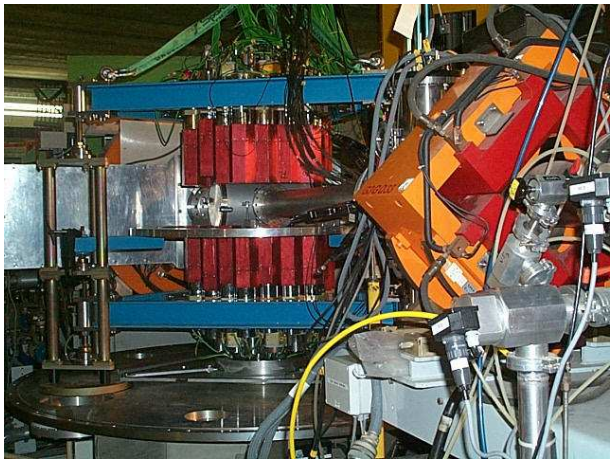

Figure 14: Chateau de Cristal

clover detectors, covering roughly 10% of the solid angle around the target, and placed in the horizontal plane of the beam, have also been included in the experiment.

The produced fragments have entered the SPEG spectrometer where they were selected and identified by the use of time-of-flight, energy loss, and focal-plane position information. Although the analysis of the coincidences between the outgoing fragments collected and identified at the SPEG spectrometer and their deexcitation γ-rays is rather complicated, the feasibility of such an in-beam γ-ray spectroscopy has been proved to be an efficient tool for nuclear structure study.

Magnesium

In the first experiment we have used a ^{36}S(77.5 A.MeV) beam with an intensity of about 1 pnA. The first results of the measurement of excited ^{30,32}Mg isotopes [A19] have shown the presence of several γ- lines.

^{32}Mg: The ^{32}Mg has confirmed the (known) excited state E(2^+) at 885 keV already measured by Motobayashi [Mot95], while the new line has an energy of 1430 keV. The $\gamma - \gamma$ coincidences have revealed that these two lines are in coincidence, and the 1430 keV line could be a $4_1^+ \rightarrow 2_1^+$ transition. Another weaker γ-ray transition has also been observed at 2870(40) keV. The analysis suggests that this transition corresponds to the direct decay of an excited state to the ground state.

^{30}Mg: The line at 1480 keV corresponds to the transition of the (known) excited state E(2^+) to the ground state. Two γ- lines at 1980 and 980 keV are with the 1480 keV transition in coincidence.

Neon

^{26}Ne: The 1660 and the 2018 keV γ-rays have already been observed in the β-delayed γ-decay of ^{26}F [A12] . The spectrum obtained by the Ge detectors shows three lines at energies 1499, 1671, and 2024 keV [A20] which are presented in Fig. 15, these γ- lines can be seen also in the spectrum from the BaF_2 detectors.

^{28}Ne: The results from in-beam spectroscopy [A20] have shown the γ-line at 1.293

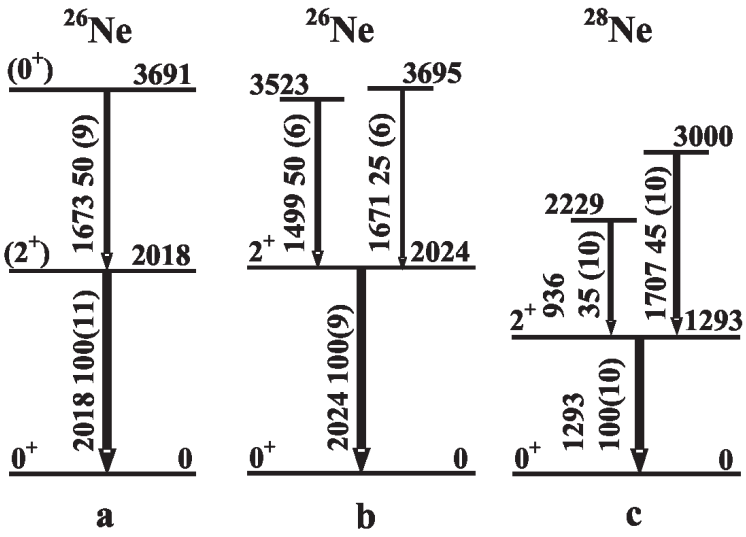

Figure 15: Nuclear levels of ^{26}Ne and ^{28}Ne; **a** - the partial level scheme of ^{26}Ne deduced in ref. [A12] from beta-decay of ^{26}F (also shown in Fig. 12); **b** - ^{26}Ne deduced from in-beam measurement [A20]; **c** - ^{28}Ne deduced from the same in-beam measurement.

MeV. Lines at 1707 and 936 keV were also observed and are shown in Fig. 15.

Oxygen

Excited states in the neutron-rich O isotopes were previously reported by Catford *et al.* [Cat89] using transfer reactions. The first excited 2^+ state of the N=14 nucleus ^{22}O is 3190 keV [Bel01, Thi00]. This is almost 2 times higher than in the adjacent N=10 and 12 nuclei and therefore indicating the presence of a N=14 (sub-) shell closure. This finding is also supported by the B(E2) value deduced from the inelastic scattering experiments [Thi00]. While the systematic trend of the first excited 2^+ states for Z=8 shows the disappearance of the N=20 shell closure, a new shell effect at N=16 has been substantiated from mass measurements and two neutron separation energies deduced from them [A13, A17].

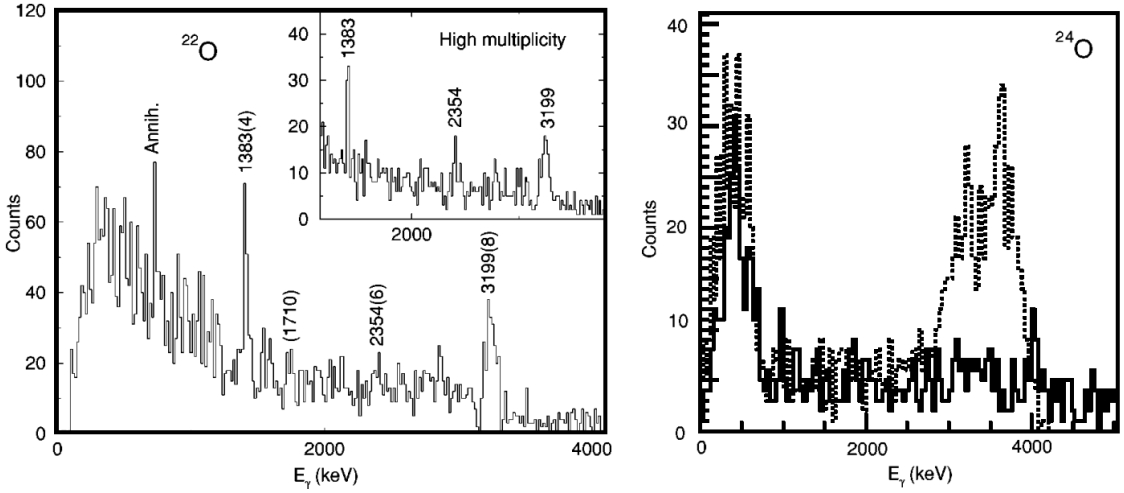

Figure 16: Doppler-corrected γ-spectra of ^{22}O (left) and ^{24}O (right).

In our papers [A21, A22] we report on first experiments probing the structure of N=12 to N=16 oxygen nuclei by use of fragmentation reactions and γ-ray spectroscopy. In the first experiment a ^{36}S(77.5 A.MeV) beam with an intensity of about 1 pnA was fragmented on a thin Be foil (2.77 mg/cm^2) located at the target place of the energy loss spectrometer SPEG at GANIL. The SPEG was tuned to the A/Z=2.75 mass to charge ratio, that is between ^{21}O and ^{22}O. As a result, the nuclei ^{20,21,22,23}O were transmitted. In addition to the BaF_2 array, four high resolution Ge detectors were used at the most backward angles. The overall Ge detector efficiency was 0.12% at 1.3 MeV. We refer to this measurement as a single step fragmentation (SSF) experiment.

In the second experiment, we used a primary beam of ^{36}S of an intensity 400 pnA on a carbon target placed in the double solenoid spectrometer SISSI. The produced nuclei were selected using the ALPHA spectrometer which magnetic rigidity and the optics of the beam line were optimized for the transmission of a cocktail beam mainly composed of fragments around ^{25,26}Ne, with energies of about 60 A.MeV. An active target composed of a plastic scintillator was used at the same place as the Be target in the SSF experiment.

This double step fragmentation (DSF) method has used two consecutive fragmentation reactions to optimize the production of the ^{24}O nuclei. Noteworthy is the fact that in the case of DSF the cocktail beam intensity can be much lower than the intensity of the ^{36}S beam. Nevertheless, ^{24}O was produced with almost a factor 10 higher intensity than it could have been produced with the SSF technique. Moreover, the raw counting rates of individual γ-ray detectors were reduced by two orders of magnitude compared to the SSF experiment.

From the level schemes proposed for ^{21}O and ^{22}O (the first 2^+ state at 3.199 MeV), as well as from the nonobservation of any γ-decay branch from ^{23}O and ^{24}O (see Fig. 16) the size of the N=14 and 16 shell gaps in oxygen isotopes could be obtained. In both cases the gaps are large and hence ^{22}O and ^{24}O are both doubly-magic nuclei. The presence of the rather well bound doubly-magic nucleus ^{24}O on the neutron drip line is a unique situation.

These results, as well all as other properties observed for ^{20,21,22,23,24}O, are in excellent agreement with predictions made nearly 20 years ago using the USD effective Hamiltonian. The T=1 part of the USD Hamiltonian, which is responsible for this behavior is essentially different from that predicted from the renormalized G-matrix and the reason for the difference is not understood. It appears that while the N=16 shell gap turns out to be larger than 3 MeV in the heaviest oxygen isotopes, it is only of the order of 1 MeV in the Si and Mg isotopes. This can be accounted for by

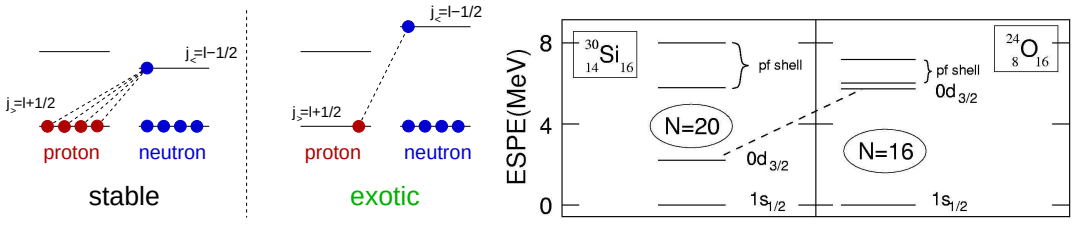

Figure 17: Schematic illustration of the strong n-p monopole interaction acting between the two spin-orbit partners $\pi 0d_{5/2}$ and $\nu d_{3/2}$.

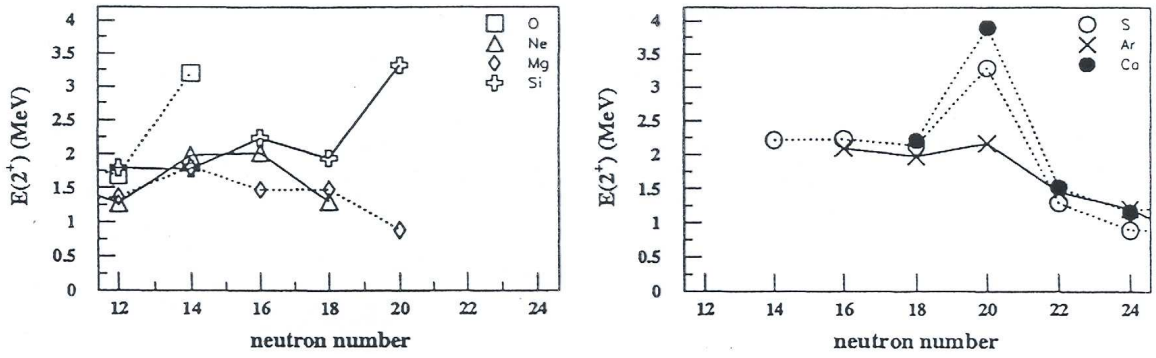

Figure 18: Dependence of E(2^+) on N for various proton numbers

considering the role of the strong n-p monopole interaction acting between the two spin-orbit partners $\pi 0d_{5/2}$ and $\nu 0d_{3/2}$ [Ots01a]. As the $d_{5/2}$ proton orbit is emptied this interaction is released and the $d_{3/2}$ neutron orbit is shifted towards the fp shell decreasing in the same time the N=20 shell gap and increasing the N=16 gap. This evolution of the neutron $d_{3/2}$ orbit is complete in the oxygen isotopes where the $\pi d_{5/2}$ is empty, making the N=16 shell gap relatively larger. Such a large N=16 gap in oxygen isotopes is probably the reason why heavier isotopes having N=18 and 20 are neutron unbound (as the $\nu d_{3/2}$ lies at higher energy than in Mg and Si nuclei). This situation is schematically presented in Fig. 17. The determination of the size of the N=16 gap in F and Ne is also important in order to complete the study of the single-particle evolution and its effect on the drip-line location in this region.

In Fig. 18 the γ-ray energies of the first 2^+ level for even-even nuclei for N ranging 12 - 24 are plotted. In the left panel first levels of ^{20}O and ^{22}O showing the steep rise to 3.2 MeV. The energy of the first 2^+ state for Ne isotopes rises from 1.25 MeV for ^{22}Ne to 2 MeV for ^{24}Ne and ^{26}Ne and then drops to 1.3 MeV for ^{28}Ne showing the flat maximum for both 14 and 16 neutron numbers and suggesting a competition between the $0d_{5/2}$ and $1s_{1/2}$ orbits as well an elimination of the N=20 shell. On the other hand, Mg isotopes show a steady decrease in the energy of 2^+ state, confirming the weakening of N=20 shell after reaching the maximum at N=14. However, Si isotopes exhibit the maxima at N=16 and 20 that suggest weakening of the N=14 subshell closure.

In the right panel of the Fig. 18 the γ-ray energies of the first 2^+ state for even isotopes of S, Ar and Ca are plotted. These nuclides exhibit pronounced maxima at N=20 shell, however, the strength of N=16 shell in these elements is very weak as these nuclides are no more neutron-rich but lie on the proton-rich side of the valley of β-stability. So we can conclude, that the strength of the N=16 shell can be observable by the in-beam γ-ray spectroscopy mainly in the region from carbon up to neon.

7 Conclusions

We can summarize main results of our experiments on nuclear halo and matter distributions:

Two-neutron halo of ^{11}Li nuclei [A1] using the elastic scattering on ^{28}Si target has been measured for the first time. To compensate for the low intensity of the radioactive neutron-rich ^{11}Li (29 A.MeV) beam, an efficient detecting system permitting one to obtain reliable experimental data has been used. An attempt to reproduce the data in DWBA and coupled-channels calculations with a double folding optical potential, with energy- and density-dependent effective interaction and realistic densities has shown the presence of a neutron-halo in ^{11}Li.

One-neutron halo of ^{11}Be [A4] has also been found in experiments of breakup reactions.

We have measured for the first time the angular distribution of the quasielastic scattering of proton halo nuclei ^{7}Be and ^{8}B (40 A.MeV) [A3] on the ^{12}C target. The Monte Carlo simulation was performed in order to carefully evaluate the efficiency of the detector setup and to estimate the experimental error bars. The shell model one-body densities and the effective interaction M3Y were used to generate the optical model potentials and the form factors for inelastic scattering. The coupled-channels calculation of quasielastic scattering accounts well for ^{7}Be while for ^{8}B the agreement is not sufficient. Instead of the proton halo these nuclei exhibit a proton skin.

A large volume of data has also been obtained for the interaction of the proton-rich ^{7}Be and ^{8}B nuclei [A5, A6] with a Si stack telescope in the energy interval 20-40 A.MeV. Only slight variations in the breakup cross sections do not confirm the predicted massive changes in the structure of these nuclei, but, on the other hand, these experiments have also confirmed the existence of the proton skin in these nuclei. The contribution to the breakup from the diffraction dissociation and absorption mechanisms were separately determined for the first time. The information about the structure of the ^{8}B nucleus is valuable not only for clarifying the question of proton halo but also for astrophysical reasons.

Very important new information collected in reaction analyses [A7] highlights the usefulness of reaction cross section measurements in assessing the relative merits of different structure and reaction models, beyond what can be inferred from elastic and inelastic scattering.

We have extracted the Coulomb and nuclear deformation lengths of ^{30,32}Mg [A8] by the inelastic excitation measurements of intermediate energy secondary beams on ^{208}Pb and ^{12}C targets. Both nuclei exhibit a similar value of $|\beta| \sim (0.5 - 0.6)$ of charge and mass deformation lengths which does not confirm predicted asymmetry in the matter distribution.

We can summarize main results of the experiments on particle stability and structure of nuclei near the neutron drip line:

In the neutron-rich region, no standard doubly-magic nuclei, neither ^{10}He [Kor94] in RIKEN nor ^{28}O [A9] in our experiment using fragmentation of the neutron-rich projectile ^{36}S(78 A.MeV) and the LISE3 spectrometer have been found. The heaviest experimentally found isotopes of carbon, nitrogen and oxygen were ^{22}C, ^{23}N and ^{24}O

with the same neutron number, N=16, [A9] while the heaviest isotope of fluorine was found to be ^{31}F with N=22 [Sak99, A11]. It is remarkable that six additional neutrons can be bound by adding just one proton to oxygen. The sudden change in stability from oxygen to fluorine may demonstrate the substantial changes in the nuclear structure in this region.

The neutron-rich isotopes ^{34}Ne and ^{37}Na were observed using the fragmentation reaction ^{48}Ca (59.8 A.MeV) + ^{nat}Ta, and thus, most probably, the neutron drip line has been reached for the neon (at N=24) and sodium (at N=26) isotopes. However, the stability of semi-magic ^{40}Mg with N=28 is very unlikely [A11].

Therefore, in the next period we concentrated to mass measurement of very neutron-rich nuclei to determine their binding energy and two-neutron separation energy which are the leading quantities to establish clear signature of nuclear shells in this region.

We have measured 31 masses of neutron-rich nuclei in the range A=29–47 [A13]. The precision of 19 masses has been significantly improved (with the uncertainty better than 1 MeV) and 12 masses were measured for the first time. The experimental shell corrections and the comparison of the measured mass excesses with models show a weakening of the N=28 shell closure which is supported by nonexistence of ^{40}Mg [A11]. In particular, the ^{43}P, ^{44}S, ^{45}Cl nuclei with N=28, appeared to be also less bound than predicted. On the other hand, there appears a discontinuity in the slope at N=26, where consequently, a pseudo-shell closure can appear. A comparison with shell model and relativistic mean field calculations demonstrates that the observed effects arise from deformed prolate ground state configurations associated with shape coexistence [A13].

However, the weakening of the N=20 shell closure for region Z$\leq$14 was also clearly seen. This complex situation of two-neutron separation energies in the O-Al region was the reason why we made an attempt to clarify the behaviour in this region. We used the fact that several particle stable nuclei [A9, Sak99, Sak96] were found to exist in this region, however, their masses are not known yet. Nevertheless, their S_{2n} values must be positive and therefore, we included the "expected" S_{2n} values of the heaviest particle stable isotopes ^{23}N, ^{22}C, ^{29,31}F and ^{31,32}Ne to the plot of two-neutron separation energies. A behaviour typical of the filling of shells which is seen at magic number N=20 has also appeared in region near N=16 for the C, N, O, F and Ne isotopes. This fact has led us to the statement about the existence of a new shell closure at N=16 [A14, A15, A16] in this neutron-rich region. Both shell closures at N=20 and N=16 are evidenced by the corresponding sharp decrease of the S_{2n} value when two neutrons are added after crossing magic numbers (N=20 and 16). After this sharp drop at the point N_{dp} (corresponding to N_{shell}+2) the S_{2n}values step down only slowly as the filling of the next shell starts to influence S_{2n}. The existence of the new shell closure at N=16 in neutron-rich nuclei is supported also by the behaviour of the calculated shell correction [A18] in the O-Al region.

The detailed inspection of neutron-rich region shows the interplay between gaps at N=8 and N=6. The gap corresponding to the N=8 is narrowing for lower Z and for Z=3 and 4 the new gap at N=6 prevails. This fact gives the evidence that instead of formerly predicted ^{10}He the really existing doubly-magic nucleus is ^{8}He. So another new shell closure has also appeared in neutron-rich nuclei at N=6 due to the push of the $0p_{1/2}$ orbit to higher energies.

Very useful way how the shell closure and magic number can be determined precisely is to measure the γ-rays emitted by excited nuclei. In-beam γ-ray spectroscopy has revealed to be an important tool to study low-lying excited states in neutron-rich nuclei, to determine the energy of the first 2^+ state for even-even nuclei, and thus to establish the gap above the ground state. The energy of the first 2^+ state for even-even nuclei of S, Si, Mg, Ne [A19, A20] and O has been measured using the Crystal ball at GANIL. The energy of the first 2^+ state of even-even nuclei exhibits the maxima at N=20 for Si, S and Ca corresponding to doubly-magic nuclei near the valley of the stability, and confirming the magic number N-20. An enhancement at N=16 for Ne, Si and S corresponding to a new neutron shell closures in neutron-rich nuclei is also visible. A special attention has been paid to measurement of oxygen isotopes $^{20-24}$O [A21, A22]. The non-observation of any γ-decay branch from ^{23}O and ^{24}O suggests that their excited states lie above the neutron decay thresholds. From this, as well as from the level schemes proposed for ^{21}O and ^{22}O, the size of the N=14 and 16 shell gaps in oxygen isotopes was discussed in the light of shell-model calculations.

This fact is strongly supported by the instability of C, N and O isotopes with N$>$ 16, and confirms the magic character of N=16 for the neutron-rich nuclei in the region 6$\leq$Z$\leq$10, while the shell closure at N=20 tends to disappear for Z$<$ 14.

We can summarize that a new shell closure at N=16 has appeared in neutron-rich nuclei for Z$\leq$10 between the $1s_{1/2}$ and $0d_{3/2}$ orbits in a good agreement with the MCSM calculations. New shell closure at N=6 which has revealed in neutron-rich nuclei for Z$\leq$4 between the $0p_{1/2}$ and $0p_{3/2}$ orbits is also in a good agreement with these calculations.

The synthesis and investigation of extremely neutron-rich isotopes are crucial for better understanding of the nature of the effective nuclear interaction. The study of the shell closures N=8, 20 and 28 is particularly interesting since their vanishing and transformation to the lower values in neutron-rich region is one of appraising facts which appeared in nuclear structure during last decade and which could be the first evidence of the changes in nuclear structure near the drip lines region.

8 References and published papers

8.1 Author's publications included to the dissertation A1-A22

[A1] M.Lewitowicz,..., Z.Dlouhy *et al.*,
Elastic scattering of a secondary ^{11}Li beam on ^{28}Si at 29MeV/n.
Nucl. Phys. **A562**, 301 (1993).
Imp. Fact.: 1.95; 46 cit.

[A2] Z.Dlouhy *et al.*,
The response of BGO scintillation detectors to light charged nuclei.
Nucl. Instr. Meth. **A317**, 604 (1992).
Imp. Fact.: 1.224; 5 cit.

[A3] I.Pecina,..., Z.Dlouhy *et al.*,
Quasielastic scattering of ^{8}B and ^{7}Be beam on the ^{12}C target at 40MeV/n.
Phys. Rev. **C52**, 191 (1995).
Imp. Fact.: 3.61; 40 cit.

[A4] F.Negoita,..., Z.Dlouhy *et al.*,
Cross sections, momentum distributions and neutron angular distributions for ^{11}Be induced reactions on silicon.
Phys. Rev. **C59**, 2082 (1999).
Imp. Fact.: 3.61; 13 cit.

[A5] F.Negoita,..., Z.Dlouhy *et al.*,
^{8}B proton halo via reaction and breakup cross section measurements.
Phys. Rev. **C54**, 1787 (1996).
Imp. Fact.: 3.61; 60 cit.

[A6] C.Borcea,..., Z.Dlouhy *et al.*,
^{8}B studied as a secondary beam at GANIL.
Nucl. Phys. **A616**, 231 (1997).
Imp. Fact.: 1.95; 3 cit.

[A7] A.de Vismes,..., Z.Dlouhy *et al.*,
Proton reaction cross-section measurements on stable and neutron-rich nuclei as a probe of the nucleon-nucleus interaction.
Nucl. Phys. **A706**, 295 (2002).
Imp. Fact.: 1.95 1 cit.

[A8] V.Chiste,..., Z.Dlouhy *et al.*,
Electric and nuclear transition strength in ^{30,32} Mg
Phys. Lett. **B514**, (2001) 233.
Imp. Fact.: 5.301; 29 cit.

[A9] O.Tarasov,..., Z.Dlouhy *et al.*,
Search for ^{28}O and study of the neutron-rich nuclei near the N=20 neutron shell closure.
Phys. Lett. **B409**, 64 (1997).
Imp. Fact.: 5.301; 63 cit.

[A10] Z.Dlouhy *et al.*,
Dripline v nuclei produced by quasi-fragmentation of the ^{32,34,36}S beams.
J. of Phys. **G25**, 859 (1999).
Imp. Fact.: 2.173; 5 cit.

[A11] S.M.Lukyanov,..., Z.Dlouhy *et al.*,
Experimental evidence for the particle stability of ^{34}Ne and ^{37}Na.

J. Phys.(London) **G28**, L41 (2002).
Imp. Fact.: 1.273; 17 cit.

[A12] A.T.Reed,..., Z.Dlouhy *et al.*,
Radioactivity of neutron-rich oxyden, fluorine ,and neon isotopes.
Phys. Rev. **C60**, 024311-1 (1999).
Imp. Fact.: 3.61; 30 cit.

[A13] F.Sarazin,..., Z.Dlouhy *et al.*,
Shape-coexistence and the N=28 shell closure far from stability.
Phys. Rev. Lett. **84**, 5062 (2000).
Imp. Fact.: 7.485; 76 cit.

[A14] Z.Dlouhy *et al.*,
Indications of changes in neutron shell closures of light very neutron-rich nuclei.
Proc. of the 9th Int. Conf. on Nuclear Mechanisms, ed. E.Gadioli Suppl.**N 115**, 651 (2000);
Czech. J. Phys. Suppl.**A 251**, 245 (2001).
Imp. Fact.: 0.360;

[A15] Z.Dlouhy *et al.*,
Characteristics of neutron-rich nuclei around shell closures N=20 and 28.
Nucl. Phys. **A701**, 189c (2002).
Imp. Fact.: 1.95; 6 cit.

[A16] Z.Dlouhy, J.Mrazek, and D.Baiborodin,
New neutron magic number N=16 far from stability.
Conf. INPC 2001, Berkeley, California, ed. E.Norman,
AIP Conf. Proc. **V610**, 736 (2002).

[A17] Z.Dlouhy,
Rearrangements in neutron shell closures far from stability.
Heavy Ion Phys. **16/1-4**, 53-64 (2002).
Imp. Fact.: 0.154

[A18] Z.Dlouhy, D.Baiborodin, J.Mrazek, G.Thiamova,
Further evidence for magic neutron number N=16 in neutron-rich nuclei.
Nucl. Phys. **A722**, 36c-41c (2003).
Imp. Fact.: 1.95; 1 cit.

[A19] F.Azaiez,..., Z.Dlouhy *et al.*,
Probing shell structure in neutron-rich nuclei with in-beam gamma-spectroscopy.
Eur. Phys. J. **A15**, 93 (2002).
Imp. Fact.: 1.659; 8 cit.

[A20] M. Belleguic,..., Z.Dlouhy *et al.*,
Search for neutron excitations across the N =20 shell gap in $^{25-29}$Ne,
Phys. Rev. **C72**, 054316 (2005).
Imp. Fact.: 3.61; 5 cit.

[A21] M.Stanoiu,..., Z.Dlouhy, *et al.*,
Study of drip line nuclei through two-step fragmentation
Eur.Phys.J. **A20**, 95 (2004).
Imp. Fact.: 1.659; 7 cit.

[A22] M.Stanoiu,...,Z.Dlouhy, *et al.*,
N = 14 and 16 shell gaps in neutron-rich oxygen isotopes,
Phys. Rev. **C69**, 034312 (2004).
Imp. Fact.: 3.61; 28 cit.

8.2 Author's publications related to the subject of the dissertation

[1] R.Anne, ..., Z.Dlouhý *et al.*, Izvestia RAN, ser.fiz. T.57, No.1 ,p.127 (1993).
[2] S.P.Tretiakova, ..., Z.Dlouhý *et al.*, Nuclear Tracks 22 (1-4), 623 (1993).
[3] A.S.Fomichev, ..., Z.Dlouhý *et al.*, Nucl. Instr. and Meth. **A344**, 378 (1994).
[4] Yu.E.Penionzhkevich, ..., Z.Dlouhý *et al.*, Nucl. Phys. **A583**, 791 (1995).
[5] Z.Dlouhý, ..., Z.Dlouhý *et al.*, Acta Polytechnica V.35 No4., 64, (1995).
[6] J.M.Corre, ..., Z.Dlouhý *et al.*, Nucl. Instr. and Meth. **A359**, 511, (1995).
[7] A.S.Fomichev, ..., Z.Dlouhý *et al.*, Z. Phys. **A351**, 129 (1995).
[8] N.Skobelev, ..., Z.Dlouhý *et al.*, Izvestia RAN, Ser. Fiz. T61, 2241, (1997).
[9] O.Tarasov, ..., Z.Dlouhý *et al.*, Nucl. Phys. **A629**, 605, (1998).
[10] A.V.Belozyorov, ..., Z.Dlouhý *et al.*, Nucl. Phys. **A636**, 419, (1998).
[11] D.V.Aleksandrov, ..., Z.Dlouhý *et al.*, Yad. Fiz. 62, No 11, 1925 (1999); Phys. Atomic Nuclei 62, 1789 (1999).
[12] J.M. Daugas, ..., Z.Dlouhý *et al.*, Phys. Lett. **B476**, 213-218 (2000).
[13] V.Chiste, ..., Z.Dlouhý *et al.*, Nucl. Phys. **A682**, 161c (2001).
[14] Z.Dlouhý, *et al.*, Czech. J. Phys., **V51**, Suppl. A, 245 (2001).
[15] W.Mittig, ..., Z.Dlouhý *et al.*, Progress of Theor. Phys. Suppl. (146): 16-22 (2002).
[16] W.Mittig, ..., Z.Dlouhý *et al.*, Eur. Phys. J. **A 15**, 157 (2002).
[17] Yu.E.Penionzhkevich, ..., Z.Dlouhý *et al.*, Eur. Phys. J. **A 13**, 123 (2002).
[18] Yu.E.Penionzhkevich, ..., Z.Dlouhý *et al.*, Yad. Fiz. **65**, 1603 (2002); Phys.Atomic Nuclei **65**, 1563 (2002).
[19] O.Sorlin, ..., Z.Dlouhý *et al.*, Phys. Rev. Lett. **88**, 092501 (2002).
[20] A.de Vismes, ..., Z.Dlouhý *et al.*, Nucl. Phys. **A706**, 295 (2002).
[21] O.Sorlin, ..., Z.Dlouhý *et al.*, Eur. Phys. J. **A16**, 55 (2003).
[22] O.Sorlin, ..., Z.Dlouhý *et al.*, Nucl. Phys. **A719**, 193c-200c (2003).
[23] H.Mach, ..., Z.Dlouhý *et al.*, Nucl. Phys. **A719**, 213c-216c (2003).
[24] G.Thiamova, ..., Z.Dlouhý *et al.*, Nuclear Physics **A719**, 312C-315C (2003).
[25] R.Fossion, ..., Z.Dlouhý *et al.*, Physic Review **C67** 2 024306 (2003).
[26] S.Grevy, ..., Z.Dlouhý *et al.*, Nucl. Phys. **A 722**, 424c-428c (2003).
[27] Z.Dlouhý, *et al.*, Phys. Atomic Nuclei **66**, 1536 (2003).
[28] M.Stanoiu, ..., Z.Dlouhý *et al.*, Eur. Phys. J.**A 22**, 5 (2004).
[29] M.Stanoiu, ..., Z.Dlouhý *et al.*, Nucl. Phys. **A746**, 135c (2004).
[30] S.Grevy, ..., Z.Dlouhý *et al.*, Nucl. Phys. **A734**, 369 (2004).
[31] S.Grevy, ..., Z.Dlouhý *et al.*, Phys. Lett. **B 594**, 252 (2004).
[32] S.Grevy, ..., Z.Dlouhý *et al.*, Nucl. Phys. **A746**, 145c (2004).
[33] J.Mrazek, ..., Z.Dlouhý *et al.*, Nucl. Phys. **A734**, E65 (2004).
[34] O.Sorlin, ..., Z.Dlouhý *et al.*, Eur. Phys. J.**A 22**, 173 (2004).
[35] V.Yu.Ugryumov, ..., Z.Dlouhý *et al.*, Nucl.Phys. **A734**, E53 (2004).
[36] H.Savajols, ..., Z.Dlouhý *et al.*, Eur. Phys. J. **A 25**, Supplement 1, 23 (2005).
[37] H.Mach,..., Z.Dlouhý *et al.*, and the ISOLDE Collaboration, Eur. Phys. J. **A 25**, Supplement 1, 105 (2005).
[38] F.de Oliveira Santos, ..., Z.Dlouhý *et al.*, Eur. Phys. J. **A 24**, 237 (2005).
[39] C.Timis,..., Z.Dlouhý *et al.*, J. Phys.(London) **G 31**, S1965 (2005).
[40] L.Gaudefroy,..., Z.Dlouhý *et al.*, Eur. Phys. J. **A 23**, 41 (2005).
[41] Khouaja,..., Z.Dlouhý *et al.*, Eur. Phys. J. **A 25**, Supplement 1, 223 (2005).
[42] J. Cerny,..., Z.Dlouhý *et al.*, Nucl. Instrum. Methods Phys. Res. **A 540**, 430 (2005).
[43] Z.Dlouhy, Acta Phys. Slovaca **56**, 91 (2006).
[44] O.Perru,..., Z.Dlouhý *et al.*, Phys. Rev. Lett. **96**, 232501 (2006).

[45] A.Khouaja,. . ., Z.Dlouhý *et al.*, Nucl. Phys. **A 780**, 1 (2006).
[46] Z.Dlouhý, *et al.*, Proc.of Int.Conf. on Exotic nuclei, Foros (1991) edt. World Scientific,Singapore (1992) 376.
[47] M.Lewitowicz, . . ., Z.Dlouhý *et al.*, Proc. of the NFFS-6 - AMCO-9 Conf. edit IOP Publishing Ltd Bristol, (1993) 337.
[48] Yu.E.Penionzhkevich, . . ., Z.Dlouhý *et al.*, Proc. of the NFFS-6 - AMCO-9 Conf., edit IOP Publishing Ltd Bristol, (1993) 345.
[49] M.Lewitowicz, Z.Dlouhý *et al.*, Proc. of 7th Int. Conf. on Nucl.Reaction Mechanisms, Varenna (June,6.-11.1994) 528.
[50] Yu.E.Penionzhkevich, . . ., Z.Dlouhý *et al.*, Proc. of the 5th Conf on N-N Collisions, Taormina (June 1994) 272.
[51] C.Borcea, . . ., Z.Dlouhý *et al.*, Proc. of the ENAM, Arles, (1995)289.
[52] M.Lewitowicz, . . ., Z.Dlouhý *et al.*, Proc. of the ENAM, Arles, (1995) 283.
[53] Yu.Penionzhkevich, . . ., Z.Dlouhý *et al.*, Proc. of the ENAM, Arles, (1995) 323.
[54] R.Anne, . . ., Z.Dlouhý *et al.*, 4 Int. Conf. on RNB, June 4-7, 1996, Omiya, Japan
[55] R.Anne, . . ., Z.Dlouhý *et al.*, 4 Int. Conf. on RNB, June 4-7, 1996, Omiya, Japan.
[56] F.Negoita, . . ., Z.Dlouhý *et al.*, 4 Int. Conf. on RNB, June 4-7, 1996, Omiya, Japan.
[57] F.Negoita, . . ., Z.Dlouhý *et al.*, 4 Int. Conf. on RNB, June 4-7, 1996, Omiya, Japan.
[58] F.Negoita, . . ., Z.Dlouhý *et al.*, Proc. of 47th Int. Symp. on Nucl. Spectr. and Structure of Atomic Nuclei, Obninsk(10-13 June,1997) 195.
[59] Z.Dlouhý, *et al.*, Proc. of 8th Int.Conf.on Nucl. Reaction Mechanisms, Varenna(June,9-14.1997) Edit. E.Gadioli, Milano Univ. (1997)416.
[60] O.Tarasov, . . ., Z.Dlouhý *et al.*, Proc. of 2nd Int.Conf. Exotic Nuclei and AtomicMasses, Michigan, USA (June 23-27, 1998).
[61] Z.Dlouhý, *et al.*, Contr. Papers of INPC, Paris (Aug., 24 - 28. 1998) p.305.
[62] F.Sarazin, . . ., Z.Dlouhý *et al.*, Contr. Papers of Int. Nucl. Phys. Conf., Paris (Aug., 24 - 28. 1998) p.423.
[63] F.Azaiez, . . ., Z.Dlouhý *et al.*, Nucl. Structure 98, Gatlinburg, Tennessee, USA (1998).
[64] A.T.Reed, . . ., Z.Dlouhý *et al.*, Proc. of 2nd Int.Conf. on Exotic Nuclei and Atomic-Masses ENAM, Michigan, USA (June 23-27, 1998).
[65] H.Savajols, . . ., Z.Dlouhý *et al.*, Proc. of 2nd Int.Conf. on Exotic Nuclei and Atomic-Masses ENAM, Michigan, USA (June 23-27, 1998).
[66] A.Gillibert, . . ., Z.Dlouhý *et al.*, Nuclear Physics in Europe facing new millennium. (June., 21 - 26. 1999), Sevilla, Spain Contr. Papers of Conf. 163 (1999).
[67] C.Borcea, . . ., Z.Dlouhý *et al.*, Proc. of 2th Int. Conf. of Exotic Nuclei and At. Masses, Michigan, ed. B.M.Sherrill, AIP 455, 278 (1999).
[68] M.Lewitowicz, . . ., Z.Dlouhý *et al.*, Nucl. Phys. **A654**, 687 (1999).
[69] F.Sarazin, . . ., Z.Dlouhý *et al.*, Proc. of 2th Int. Conf. of Exotic Nuclei and At. Masses, Michigan, ed. B.M.Sherrill, AIP 455, 44 (1999).
[70] R.G.Allatt, . . ., Z.Dlouhý *et al.*, Proc. of 2th Int. Conf. of Exotic Nuclei and At. Masses, Michigan, ed. B.M.Sherrill, AIP 455, 570 (1999).
[71] A.T. Reed, . . ., Z.Dlouhý *et al.*, Proc. of 2th Int. Conf. of Exotic Nuclei and At. Masses, Michigan, ed. B.M.Sherrill, AIP 455, 572 (1999).
[72] Z.Dlouhý, *et al.*, Proceedinngs on the 9th Int. Conf. on Nuclear Reaction Mechanisms, Ed. by E.Gadioli (5.- 9. June, 2000), Varenna, Italy, Supplemento N.115,651-660 (2000).
[73] Z.Dlouhý, *et al.*, Int. Symp. on Perspectives in Physics with RIB2000 (13.- 16.Nov., 2000) Hayama, Kanagawa, Japan, C-12.(2000).
[74] Z.Dlouhý, *et al.*, Zbornik prispevkov 13. Konf. slovenských a ceských fyziku (23.- 26. Aug., 1999), Zvolen, Slovensko, Ed. M.Reiffers, L.Just SFS , 52-55 (2000).

[75] Z.Dlouhý, *et al.*, Proc. of 4th Int. Workshop on Laser Spectr. of Rad. Nucl. Beams (May, 24 - 27. 1999) Pozna, Poland, Ed. B.Markov, Dubna JINR 156-160, (2000).
[76] A.de Vismes, ..., Z.Dlouhý *et al.*, RNB2000, 5th Int. Conf. on Radioactive nuclear beams (3.- 8.Apr. 2000) Divonne, Francie, Abstracts, S1.No 16.(2000).
[77] Z.Dlouhý, *et al.*, Int.Symp. on Nuclear Structure Physics (5.- 8.March., 2001), Goettingen,Germany, 345 (2001).
[78] H.Mach, ..., Z.Dlouhý *et al.*, Int. Symp. on Nuclear Structure Physics (5.- 8.March., 2001), Goettingen, Germany, 379 (2001).
[79] J.Mrazek, ..., Z.Dlouhý *et al.*, Int.Symposium on Exotic Nuclei, Baikal Lake, (July24-28, 2001) Contributions, 29, (2001).
[80] D.Baiborodin, ..., Z.Dlouhý *et al.*, Int.Symposium on Exotic Nuclei, Baikal Lake, (July24-28, 2001) Contributions, 30, (2001).
[81] Z.Dlouhý, *et al.*, Proc of IV Latin American Symposium on Nuclear Physics Mexico D.F.,Mexico (Sept 24-28, 2001) UNAM, 19 , (2001).
[82] Z.Dlouhý, *et al.*, Nuclear Phys. in the 21st Century, Int.Nucl. Phys. Conf. INPC 20001, Ed.E.Norman, L.Schroeder, and G.Wozniak, LBNL, Berkeley, California, AIP Conf. Proc. V 610 736 (2002).
[83] N.L.Achouri, ..., Z.Dlouhý *et al.*, Proc. of Int.Conf. of Nuclear Physics at Border Lines, ed.Fazio et al. World Sci., 30 (2002).
[84] Z.Dlouhý, *et al.*, Proc. of Int.Conf. of Nuclear Physics at Border Lines, ed.Fazio et al. World Sci., 85 (2002).
[85] O.Sorlin, ..., Z.Dlouhý *et al.*, Proc. of Int.Conf. of Nuclear Physics at Border Lines, ed.Fazio et al. World Sci., 322 (2002).
[86] Z.Dlouhý, *et al.*, VII Int. School-Seminar on Heavy Ion Physic, (May 27-Jun 1, 2002) FLNR- JINR Dubna, 88 (2002).
[87] Z.Dlouhý, *et al.*, 11th Int. Symposium on Capture Gamma-Ray Spectroscopy and Related Topics, Pruhonice, Sept. 2 - 6, 2002.
[88] Z.Dlouhý *et al.*, Proc of 3th Int. Conf. On Fission and Properties of Neutron-Rich Nuclei, Nov. 3-9, 2002 Sanibel Island, Florida, 18(2002).
[89] H.Mach, ..., Z.Dlouhý *et al.*, 11th Int. Symposium on Capture Gamma-Ray Spectroscopy and Related Topics, Pruhonice, Sept. 2 - 6, 2002.
[90] H.Mach, ..., Z.Dlouhý *et al.*, 17th Int. Nuclear Physics Divisional Conference of EPS (Sept. 30.- Oct. 4, 2002), Debrecen, Hungary , 50 (2002).
[91] O.Sorlin, ..., Z.Dlouhý *et al.*, Proc.Frontiers of Nuclear Structure, Berkeley, California, P.Fallon and R.Clark, Eds., p.311 (2003); AIP Conf.Proc. 656 (2003).
[92] H.Mach, ..., Z.Dlouhý *et al.*, Proc. of the 11th Int. Symp. Capture Gamma Ray Spectroscopy and RElated Topics, ed. J. Kvasil, World Sci., 476 (2003).
[93] G.Thiamova, ..., Z.Dlouhý *et al.*, Proc. of the 11th Int. Symp. Capture Gamma Ray Spectroscopy and RElated Topics, ed. J. Kvasil, World Sci., 837 (2003).
[94] Z.Dlouhý, *et al.*, Nuclei at LIMITS 04, (Jul 26- 31, 2004), Argonne, USA, P26 (2004).
[95] Z Dlouhy, *et al.*, ENAM 2004, (Sept. 12-16, 2004) Georgia, USA.
[96] Z.Dlouhý, *et al.*, Proc of 15-th Conference of Czech and Slovak Physicist, Kosice, Slovakia, September 5-8, 2005.
[97] Z.Dlouhý, *et al.*,FINUSTAR Sept.12-17,2005 Kos, Greece, AIP Conf. Proc. V 815 442 (2006)
[98] J.C.Angelique, ..., Z.Dlouhý *et al.*, FINUSTAR Sept.12-17,2005 Kos, Greece, AIP Conf. Proc. V 815 134 (2006)
[99] A.Buerger, ..., Z.Dlouhý *et al.*, FINUSTAR Sept.12-17,2005 Kos, Greece, AIP Conf. Proc.V 815 418 (2006) .

8.3 Other references

[Ann92] R. Anne *et al.*, Nucl. Instr. Meth. **B70** 276 (1992).
[Aud97] G. Audi *et al.*, Nucl. Phys. **A624** 1 (1997).
[Bar95] F. C. Barker, Nucl. Phys. **A588**, 693 (1995).
[Bau01] E. Bauge, J.P. Delaroche, M. Girod, Phys. Rev. C 63 (2001)024607.
[Bec69] F.D. Becchetti, G.W. Greenlees, Phys. Rev. **182** 1190 (1969).
[Bel01] M. Belleguic *et al.*, Nucl. Phys. A682, 136c (2001).
[Ber77] G.F. Bertsch, J. Borysowicz, H. McManus,W.G. Love, Nucl. Phys. A 284, 399 (1977).
[Ber89] G.F. Bertsch, B.A. Brown and H. Sagawa, Phys. Rev. C39 (1989) 1154.
[Bro96] A. Brown, A. Csoto, and R. Sherr, Nucl.Phys. **A597**, 66 (1996).
[Bro98] B.A. Brown, Phys. Rev. **C58** 220 (1998).
[Cat89] W.N. Catford *et al.*, Nucl. Phys. **A503**, 263(1989).
[Cau98] E. Caurier et al., Phys. Rev. C 58 2033(1998).
[Die85] F.S. Dietrich, F. Petrovich, in: Proc. AIP, V 124, New York, 1985, p.90.
[Dlo92] Z. Dlouhy *et al.* Proc. 6 Int.Conf. on NFFS, Berncastel-Kues,Germany, p.481, (1992).
[End90] P.M. Endt, Nucl. Phys.**A521**, 1, (1990).
[Fau96] M. Fauerbach *et al.*, Phys. Rev.**C53** 647 (1996).
[Fuk92] N. Fukunishi, T. Otsuka, T. Sebe, Phys. Lett. B 296 279(1992).
[Gil87] A. Gillibert *et al.*, Phys. Lett. **B192** 39 (1987).
[Gui90] D. Guillemaud-Mueller *et al.*, Phys. Rev. **C41** 937 (1990).
[Han87] P.G. Hansen and B. Jonson, Europhys. Lett. **4** 409 (1987).
[Hax49] O. Haxel, J.H.D. Jensen and H.E. Suess, Phys.Rev.**75** 1766 (1949).
[Hon95] M. Honma, T. Mizusaki and T. Otsuka, Phys. Rev. Lett. **75** 1284 (1995).
[Hon96] M. Honma, T. Mizusaki and T. Otsuka, Phys. Rev. Lett. **77** 3315 (1996).
[JLM77] J.P. Jeukenne, A. Lejeune, C. Mahaux, Phys. Rev. **C16** 80 (1977).
[Kny81] O.M. Knyazov, E.F. Hefter, Z. Phys. A 301, 277 (1981).
[Kor94] A. Korsheninnikov *et al.*, Phys. Lett. **B326** 31 (1994).
[Kuo68] T.T.S.Kuo and G.E. Brown, Nucl. Phys. **A114** 241 (1968).
[Lop99] M.J.Lopez *et al.*, Preprint GANIL P 99 08
[Min92] T. Minamisono *et al.*, Phys. Rev. Lett. **69** 2058(1992).
[Mit97] W. Mittig, A. Lepine-Scilly and N. Orr, Annu. Rev. Nucl. Sci. **47** 27 (1997).
[Miz96] T. Mizusaki, M. Honma and T. Otsuka, Phys. Rev. **C53** 2786 (1996).
[Mol95] P. Möller and J.R. Nix, At. Data Nucl. Data Tables **59** 85 (1995).
[Mot95] T. Motobayashi *et al.*, Phys. Lett. **B346** 9 (1995).
[Orr89] N.A. Orr, L.K. Fifield, W.N. Catford, and C.L. Woods, Nucl. Phys. **A491** 457 (1989).
[Orr91] N.A. Orr *et al.*, Phys. Lett. **B258** 29 (1991).
[Ost94] A.N. Ostrowski *et al.*, Phys. Lett. **B338** 13 (1994).
[Ots98] T. Otsuka, M. Honma and T. Mizusaki, Phys. Rev. Lett. **81** 1588 (1998).
[Ots01] T. Otsuka *et al.*, Nucl. Phys. **A685** 100c (2001).
[Ots01a] T. Otsuka *et al.*, Phys. Rev. Lett. **87** 082502 (2001).
[OXB88] B. A. Brown *et al.*, MSUNSCL Report No.524 (1988).
[Oza00] A. Ozawa *et al.*, Contr. to RNB2000, 3-8 April 2000, Divonne(France);
Phys. Rev. Lett. **84** 5493 (2000).
[Pak01] A. Pakou *et al.*, Nucl. Phys. **A691** (2001) 661.
[Pov87] A. Poves and J. Retamosa,Phys. Lett. **B184** 311 (1987).
[Pov94] A. Poves and J. Retamosa, Nucl. Phys. **A571** 22 (1994).
[Pri99] B.V. Pritychenko *et al.*, Phys. Lett. B 461 322(1999).
[Ret97] J. Retamosa *et al.*, Phys. Rev. **C55** 1266 (1997).
[Sak96] H. Sakurai *et al.*, Phys. Rev. **C54** R2802 (1996).
[Sak99] H. Sakurai *et al.*, Phys. Lett. **B448** 180 (1999).

[Sam97] C. Samanta,*et al.*, J. Phys. G 23, 1697 (1997) and references therein.
[Sat79] G.R. Satchler, W.G. Love, Phys. Rep. **55** 184 (1979).
[Sat83] G.R. Satchler, Direct Nuclear Reactions, (Oxford University Press, New York, 1983).
[Ste88] J. Stevenson *et al.*, Phys. Rev. **C37** 2220 (1988) and ref. therein.
[Ste02] P.D. Stevenson, J. Rikovska Stone, M.R. Strayer, Phys.Lett. 545B, 291 (2002).
[Suz95] T. Suzuki *et al.*, Phys. Rev. Lett. **75** 3241 (1995).
[Suz98] T. Suzuki *et al.*, Nucl. Phys. **A630** 661 (1998).
[Tan85] I. Tanihata *et al.*, Phys. Rev. Lett. **55** 2676 (1985).
[Tan88] I. Tanihata *et al.*, Phys. Lett.**B206** 592 (1988).
[Ter97] J. Terasaki *et al.*, Nucl. Phys. **A 621** 706(1997).
[Thi75] C. Thibault *et al.*, Phys. Rev. **C12** 644 (1975).
[Thi00] P.G. Thirolf *et al.*, Phys. Lett. **B485** 16 (2000).
[Uts99] Y. Utsuno, *et al.*, Phys. Rev. **C60** 154315-1 (1999).
[Vau72] D. Vautherin and D.M. Brink, Phys. Rev. C5(1972) 626.
[Vis01] A.de Vismes et al., Phys. Lett. B 505 (2001) 15.
[War90] E.K. Warburton *et al.*, Phys. Rev. **C41** 1147 (1990).
[WaB92] E.K. Warburton and B.A. Brown, Phys. Rev. **C46** 923 (1992).
[Wil84] B.H. Wildenthal, Prog. Part. Nucl. Phys. 11, 5 (1984).